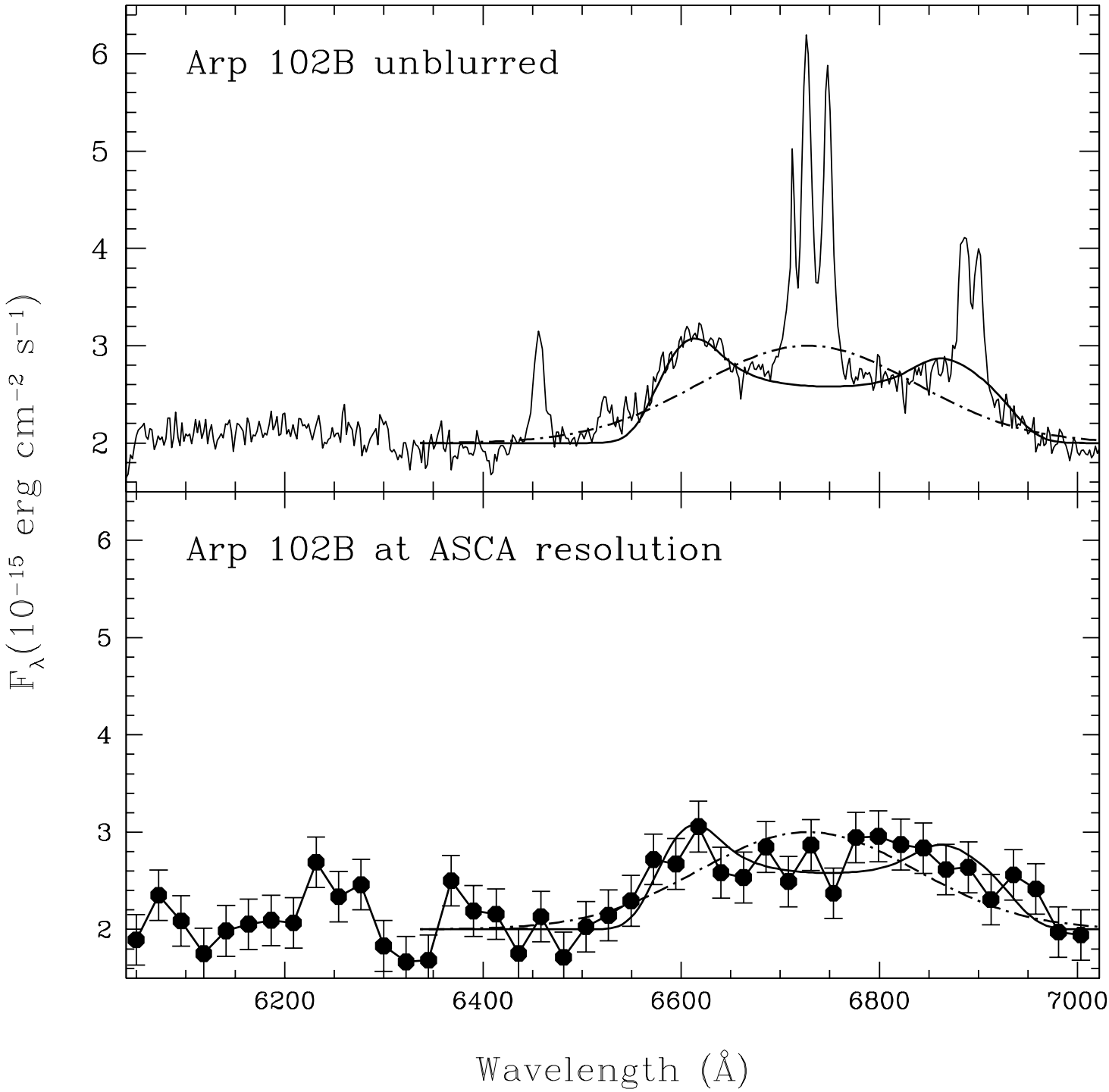
Arp 102B unblurred
Arp 102B at ASCA resolution
$F_\lambda (10^{-15}$ erg cm^{-2} s$^{-1})$
Wavelength (Å)
2
3
4
5
6
6200
6400
6600
6800
7000

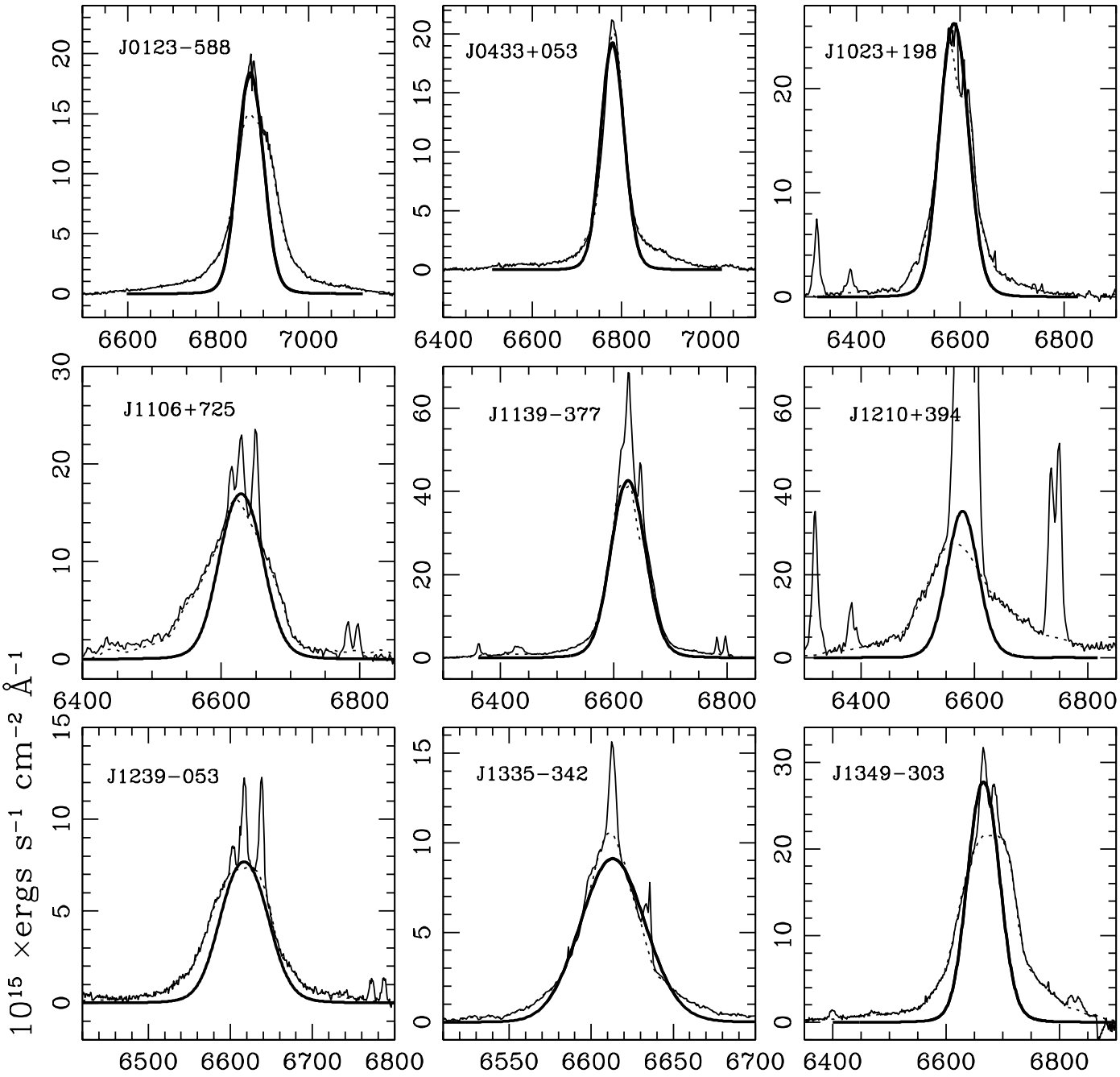
J0123−588
J0433+053
J1023+198
J1106+725
J1139−377
J1210+394
J1239−053
J1335−342
J1349−303
10^{15} ×ergs s^{-1} cm^{-2} Å^{-1}

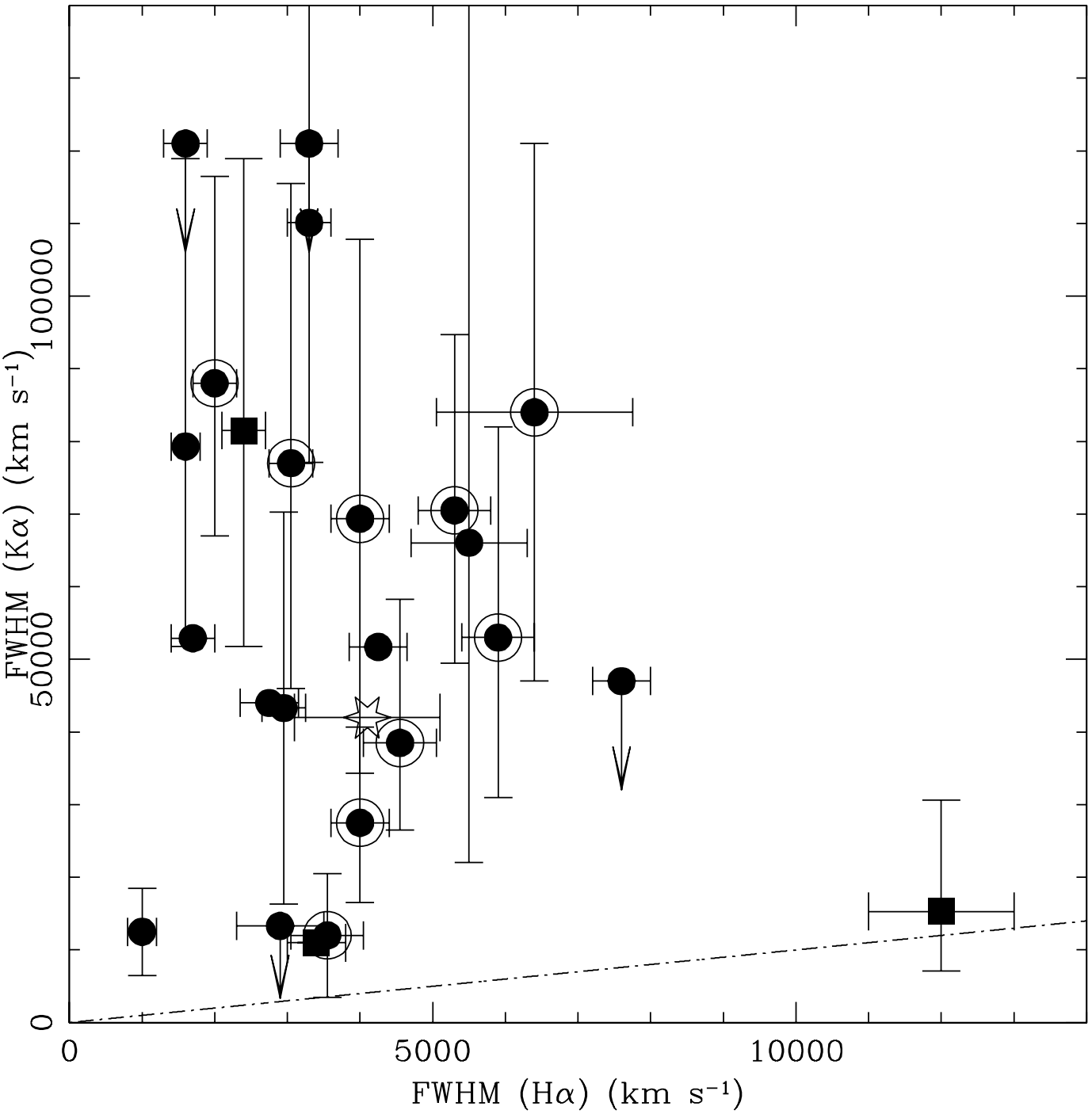
FWHM (Kα) (km s⁻¹)
0
50000
100000
0
5000
10000
FWHM (Hα) (km s⁻¹)

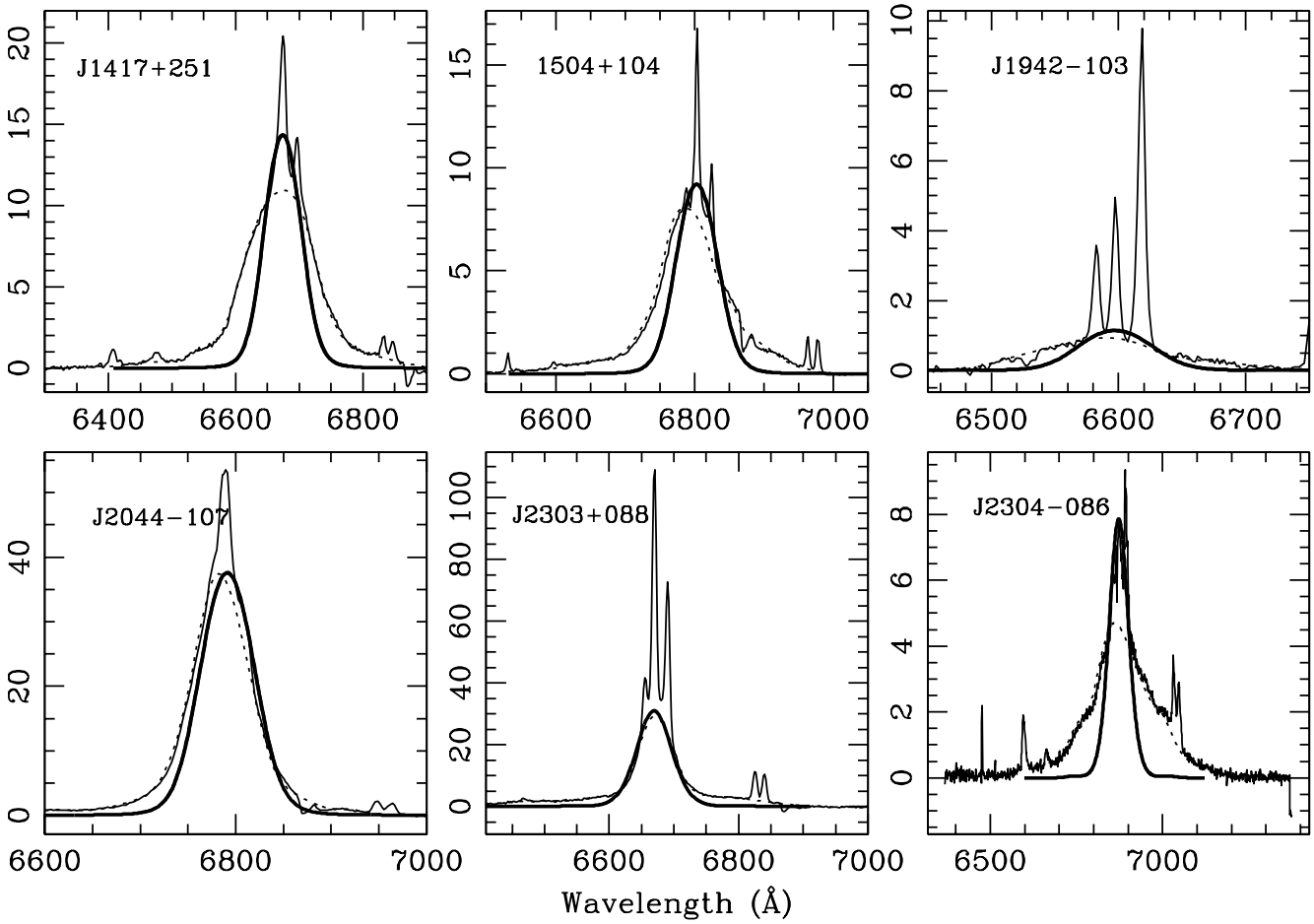
J1417+251
1504+104
J1942−103
J2044−107
J2303+088
J2304−086
Wavelength (Å)

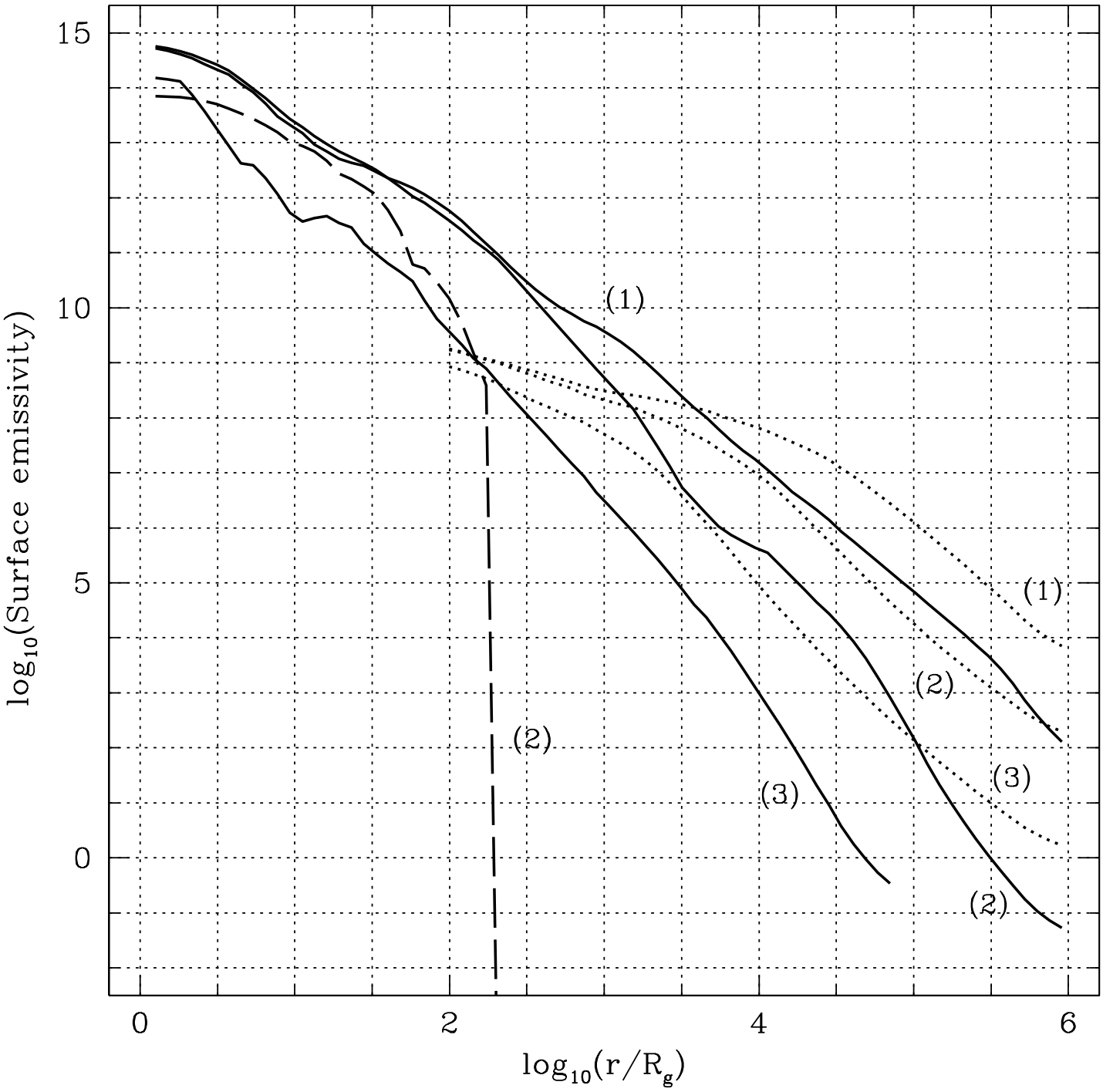
15
10
5
0
0
2
4
6
log10(Surface emissivity)
log10(r/Rg)
(1)
(2)
(3)
(1)
(2)
(3)
(2)

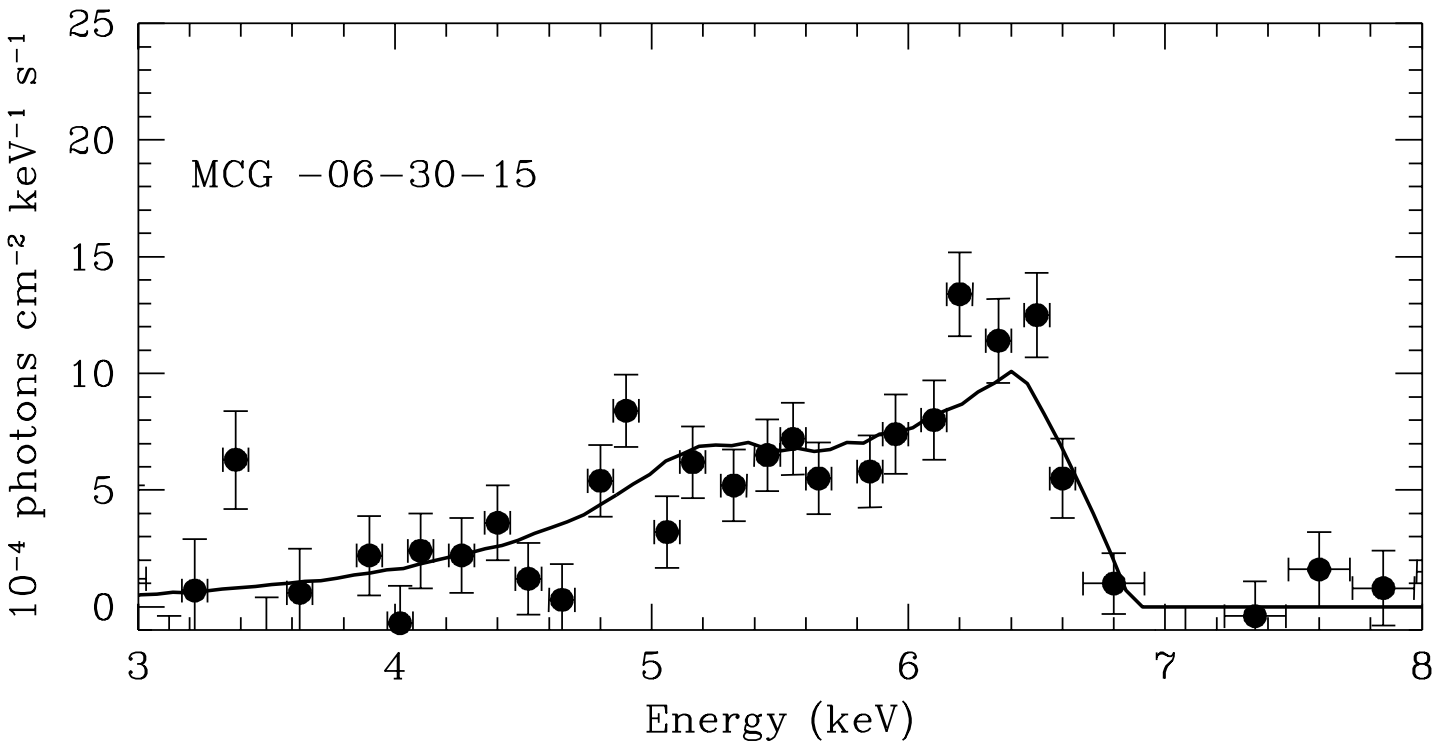
MCG −06−30−15
10⁻⁴ photons cm⁻² keV⁻¹ s⁻¹
Energy (keV)
0
5
10
15
20
25
3
4
5
6
7
8

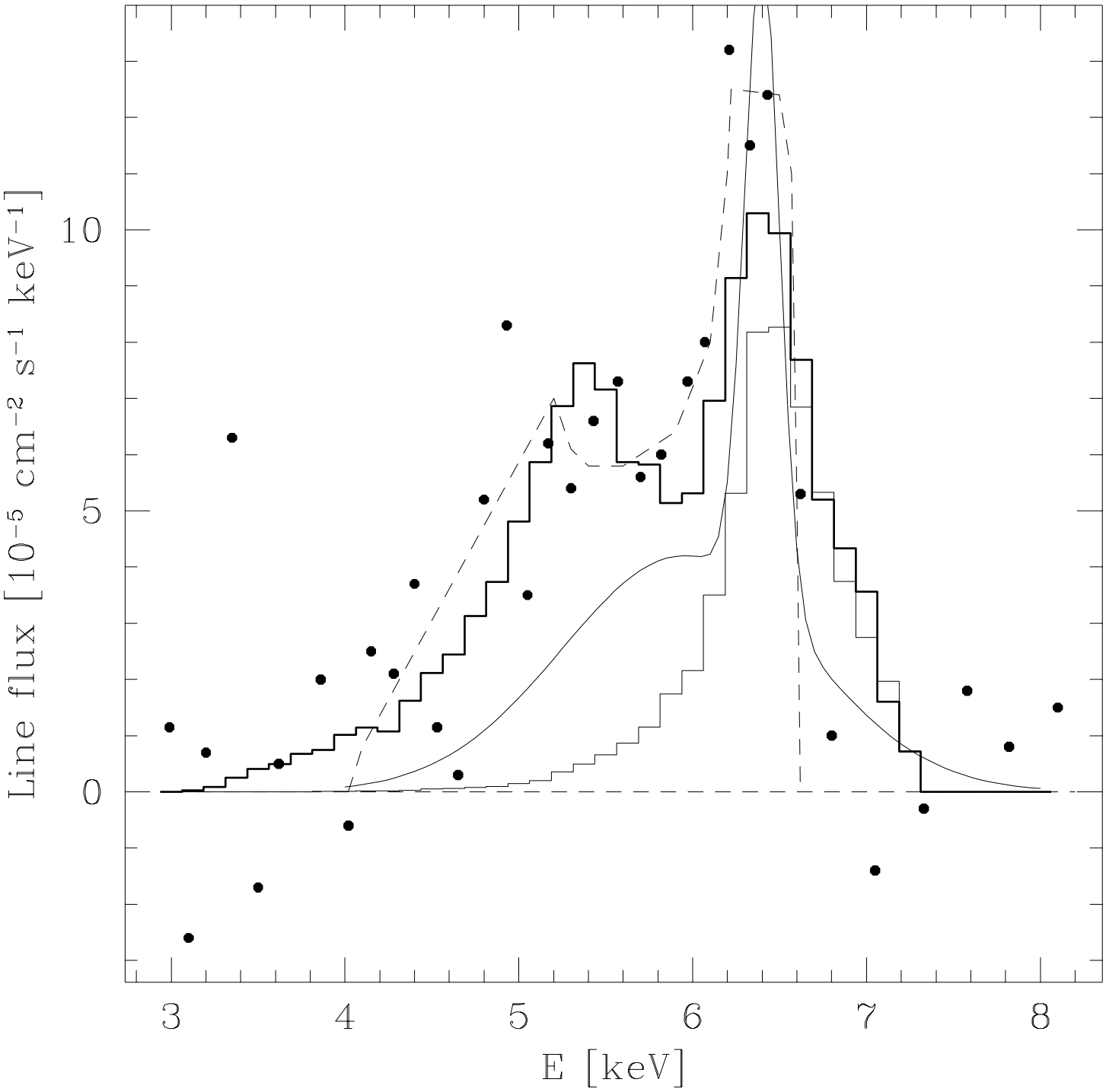
Line flux [10^{-5} cm^{-2} s^{-1} keV^{-1}]
10
5
0
3
4
5
6
7
8
E [keV]

arXiv:astro-ph/9712336v1 29 Dec 1997

On the Origin of Broad Fe Kα & Hi Hα Lines in AGN[1]

J. W. Sulentic[2], P. Marziani[3,4], T. Zwitter[5], M. Calvani[3] and D. Dultzin-Hacyan[4]

ABSTRACT

We examine the properties of the Fe emission lines that arise near 6.4 keV in the ASCA spectra of AGN. Our emphasis is on the Seyfert 1 galaxies where broad and apparently complex Fe Kα emission is observed. We consider various origins for the line but focus on the pros and cons for line emitting accretion disk models. We develop a simple model of an illuminated disk capable of producing both X-ray and optical lines from a disk. The model is able to reproduce the observed Fe Kα FWHM ratio as well as the radii of maximum emissivity implied by the profile redshifts. The overall profile shapes however do not fit well the predictions of our disk illumination model nor do we derive always consistent disk inclinations for the two lines. We conclude that the evidence for and against an accretion disk origin for the Fe Kα emission is equal at best. The bulk of the data requires a very disparate set of line fits which shed little light on a coherent physical model. We briefly consider alternatives to disk emission models and show that a simple bicone model can reproduce the Fe line profiles equally well.

Subject headings: Galaxies: Active – Galaxies: Kinematics & Dynamics – Galaxies: Nuclei – Galaxies: Seyferts – Galaxies: Emission Lines – Galaxies: X–Rays – Line: Formation – Line: Profiles

---

[1]Based in part on observations collected at ESO, La Silla

[2]Department of Physics & Astronomy, University of Alabama, Tuscaloosa, AL 35487, USA. E-mail: giacomo@merlot.astr.ua.edu

[3]Osservatorio Astronomico, Padova, Italy

[4]Instituto de Astronomia, UNAM, Mexico City, DF 04510, Mexico

[5]Department of Physics, University of Ljubljana, Ljubljana, Slovenia

1. Introduction

The idea that a significant fraction of the broad line emission in Active Galactic Nuclei (AGN) comes directly from an accretion disk is attractive for several reasons beyond the obvious one of proving the black hole paradigm. The disk provides a high density medium where the integrated intensities of the optical FeII lines can be accounted for. An illuminated disk can also more easily produce the strong Balmer lines (i.e. the Lα/Hβ problem: see Collin-Souffrin & Dumont 1990). Apparent density and kinematic differences between high and low ionization lines (Gaskell 1982; Sulentic 1989) can also be explained if the latter arise from a disk. Naturally there was considerable excitement when the double-peaked Balmer lines in Arp102B were discovered (Chen, Halpern and Filippenko 1989). The line profiles in that AGN could be well-fit by the predictions of a model for line emission from a relativistic Keplerian disk (Chen and Halpern 1989). The fit to Arp102B was quite good but the statistical implications were not. The best disk model fits to lines in Arp102B imply an intermediate viewing angle and that leads to the expectation of many sources with double-peaked emission lines. A search for more double peaked and peculiar profiles among radio-loud AGN revealed only a handful that could be reasonably well fit by disk models (Eracleous and Halpern 1994).

AGN with optical line profiles like Arp102B are apparently quite rare. They also appear to be almost uniquely radio-loud sources. Either most radio-loud disk emitters (and all radio-quiet ones) produce emission at larger radii where double peaked lines are not expected or the disk contribution to the broad line emission is small or negligible. The unsatisfactory alternative would be that we are viewing virtually all AGN aligned with the disk axis near pole-on. A comparison between line profile shifts/asymmetries with disk model predictions (Sulentic et al. 1990) suggests that at least part of the line emission in most quasars must arise from another source. This conclusion is based on the large number of line profiles that show blue shifts and/or blue asymmetries (implying that the red side of the profile is brighter) in conflict with disk model predictions. Even the most promising double-peaked sources (e.g. Arp102B, 3C390.3) require fine tuning of the disk models (see e.g. Gaskell 1996; Zheng et al. 1991) because the profile peaks appear to vary out of phase. A new double peaked source arose in Pictor A with first a red, and then a blue, peak developing over a five year period (Sulentic et al. 1995a). Such variations and the overall rarity of double-peaked profiles appear to be more easily explained with models invoking a predominance of radial motion. Such models also have the advantage that they can directly account for the rarity of peculiar line profiles because such profiles would arise at an extremum in the orientation/kinematic domain (Sulentic et al. 1995a).

A possible kinematic difference between high and low ionization lines (HIL and LIL;

HIL include CIVλ1549 and HEII lines; LIL are Balmer lines, FEII$_{\rm opt}$ lines, and MGIIλ2800) was one of the reasons that models for a two zone broad line region (disk + something else) became necessary and popular. The evidence revolves around a possible systematic blueshift of the HIL with respect to the LIL (the LIL showing centroid velocities similar to the source rest frame). The most peculiar line profiles were found in the radio-loud AGN population and subsequent searches for disk candidates focused there (Eracleous and Halpern 1994). Ironically the largest sample yet studied for line profile shifts indicates that it is only the *radio-quiet* AGN that show a systematic HIL blueshift with respect to the LIL (Sulentic et al. 1995b; Marziani et al. 1996).

Recent advances in X-ray spectral resolution offered by the Advanced Satellite for Cosmology and Astrophysics (ASCA; Tanaka, Holt, & Inoue 1994) provide a possible new form of evidence for disk emission in (predominantly) radio-quiet AGN. We may be observing the very innermost regions of the disk that could be producing an iron Kα line by Compton reflection or photo-ionization (e. g. Tanaka et al. 1995; Fabian et al. 1995; Dabrowski et al. 1997; Fanton et al. 1997). Strong and broad line emission is often observed near 6.4 keV in AGN spectra (Mushotzky, Done, & Pounds 1993; Mushotzky 1997; Nandra et al. 1997a,b, and references therein). Figure 1 illustrates the difficulties that we face in quantifying the X-ray line emission. While ASCA provides a tremendous advance in X-ray spectroscopy, the resolution (2-5% at 6 keV) and S/N obtainable still lag far behind optical data. We show a typical modern observation of the Hα line profile for Arp102B degraded to the resolution and S/N of a typical ASCA spectrum. Narrow lines near Hα arising from [NII]$\lambda\lambda$6548,6583, [OI]λ6300 and [SII]$\lambda\lambda$6717,6730 were removed from the spectrum before blurring because the FE Kα emission in AGN has no known analogous contaminants, albeit FE Kα might involve a blend of multiple, broad and narrow, components. While optical observations can discriminate between a disk model and a broad gaussian, ASCA observations cannot (see Fig. 1).

We consider FE line detection statistics for different AGN classes in § 2. In § 3 we consider an accretion disk origin for the FE Kα and HI Hα lines. In § 3 we model an illuminated disk (e.g. Dumont & Collin-Souffrin 1986) to account for both optical and X-ray emission lines simultaneously. In § 4 we summarize problems with the accretion disk interpretation for FE Kα and consider an alternative model for the X-ray line emission.

2. X-ray and Optical Observations

The energy of the emitted FE Kα depends on ionization stage. The ASCA resolution allows us to distinguish line emission from three main ranges of ionization: (1) emission

from neutral or weekly ionized iron ("cold iron" emission; ionization stage $\leq$FeXVIII), as expected from cold, dense gas in an accretion disk; (2) emission from mildly to highly ionized iron at 6.45 keV $\lesssim$ energy $\lesssim$ 6.7 keV, for FeXIX$\leq$ ionization stage $\leq$FeXXV; (3) emission from H-like Fe at 6.97 keV (FeXXVI). The most robust measurement is the centroid energy of the line, but even this can become confused when the line is broad. Determination of the profile width, asymmetry index or equivalent width are more difficult and model dependent. These parameters, and the derived χ^2 goodness-of-fit are quite sensitive to the continuum fit which includes a basic power law modified by both emission and absorption processes (correlated to the line itself).

2.1. Statistics of Emission lines near 6.4 keV

Table 1 summarizes the published Fe line parameters for most AGN with detected Fe Kα emission in ASCA spectra. The list should be reasonably complete through 1996. The format for Table 1 is as follows: Column 1 - abbreviated (2000) position taken from the 7th edition of the Veron & Veron catalog; Column 2 - a common name for the source as used in the ASCA-related literature; Column 3 - AGN type; Column 4 - optically determined redshift; Columns 5, 6, and 7 - the derived Fe Kα line peak centroid energy, profile Gaussian width (keV) and EW (eV), respectively; Column 8 - reference(s) to the source of the Fe Kα parameters given in the three previous columns. Table 1 reflects the best currently derived line parameters. In some cases a range is given to reflect a range of reasonable solutions, providing additional insight into the uncertainties associated with these numbers. References should be consulted for details of adopted continuum and line properties. We focus our discussion on the Seyfert galaxies because: (1) that is where the largest body of X-ray emission line data exists and the statistics of Fe Kα emission from broad-line radio galaxies and quasars are not yet clear and (2) the Fe Kα spectra of Sy 1 galaxies sometimes show "disk-like" profiles.

A recent study by Nandra et al. (1997a,b) has collected much of the data and reduced it uniformly. The best model fits to Seyfert 1 spectra always show Fe emission with approximately 80% of the detections better fit by a resolved broad line. Nandra et al. (1997b) find a distribution of profile (Gaussian fit σ) widths with: (1) about half of the sample clustered at 0.7$\pm$0.1 keV and (2) the other half of the sample extending continuously from 0.5 keV down to unresolved instrumental width ($\sim$0.1 keV). The profiles frequently show a narrow component centered very near to 6.4 keV accompanied by an asymmetry towards the red. In several cases the spectra suggest a multicomponent structure within this red wing rather than a smooth extension. In most cases it is impossible to determine

if this multicomponent structure is real or due to instrumental effects and low S/N. The distribution of line equivalent widths extends from 50-600 eV with a mean EW∼160. Typical uncertainties for the individual estimates cover most of this range. The major point of consensus is that we typically observe a broad component extending 1-1.5 keV to the red of a narrow peak that is centered very close to 6.4 keV. The two simplest models of the line involve: (1) a single asymmetric feature (§ 3) or (2) a combination of two symmetric features one narrow/unshifted and another broad/redshifted (§ 4).

The situation for radio quiet quasars is very confused with many showing no evidence of rest frame emission near 6.4 keV. At the same time sources from 3C273 to S5 0014+813 (Elvis et al. 1994) at z=3.384 show evidence for a line. Rest frame centroid energies for these detections range from 6.4-6.9keV. Few observations for radio-loud sources have been published and the situation is not clearly defined. No radio-loud sources as yet show broad Fe profiles like IRAS18325-5926 or Sy 1's, as further discussed in § 2.2. In 3C390.3 (Eracleous et al. 1996) the Hα and Kα widths are similar while for 3C120 Fe Kα may show either a single broad line or 3 individual narrower features. A recent observation for Pictor A (Halpern et al. 1997) shows no Fe line. Recent claims (Reynolds 1997) that radio loud sources show much broader Fe Kα profiles than radio quiets are based upon very broad and uncertain detections for 3C120 and 3C382.

Seyfert 2 sources usually show narrow Fe Kα emission. The results from a large GINGA sample (Smith & Done 1996) indicate that most lines have a centroid near 6.4 keV with a subset centered between 6.6-7.0 keV. In two of the best studied cases (Mark 3 and NGC1068) there is evidence for both neutral and ionized Fe lines, possibly components of FeII emission from all three ionization ranges listed above. The most unusual Sy2 sources are IRAS 18325-5926 and MCG-5-23-16 where very broad lines were detected. The former source shows a broad (spanning 4.5–7 keV) profile, red (low energy) asymmetry and narrow peak on the blue (high energy) side centered at 6.8 keV. It is unclear whether this is a single line or a blend of several features but it is reasonably certain that the extended emission redward of 6.4keV is real. MCG-5-23-16 shows a broad component extending from 5–8 keV with a narrow peak near 6.4 keV. Multiple components are again a distinct possibility. The "hidden" quasar IRAS 09104+4109 (Fabian et al. 1994b) has been proposed as an ultraluminous example of the Sy2 class. It shows a very strong but narrow Fe line centered at 6.65 keV.

2.2. BLR Hα Statistics and Comparison with Fe Kα

We have obtained, or gained access to, optical spectra for almost every Seyfert 1 galaxy that shows a strong Fe Kα (ASCA) detection so far. Observations that have not been presented elsewhere are summarized in Table 2. The format is as follows: Column 1 - abbreviated IAU designation; Column 2 - other name; Column 3 - date of observation; Column 4 - universal time of observation; Column 5 - exposure time in seconds; Column 6 - observatory; Column 7 - telescope; Column 8 - spectrograph; Column 9 - grating and Column 10 - resolution FWHM (in Å).

Table 3 summarizes the HI Hα profile properties for both old and new observations. The format is as follows: Column 1 - IAU code name; Column 2 - source name; Column 3 - Seyfert type; Column 4 - EW in Å; Column 5 - FWHM in km/s; Column 6 - uncertainty at $2\times\sigma$ confidence level; Column 7 - centroid line shift (at half maximum) in km s^{-1}; Column 8 - line centroid uncertainty; Column 9 - reference code. Uncertainty of Hα EW values should be $\approx 10\%$. Figure 2 shows a comparison of Hα and Fe Kα profile FWHM values. The values plotted for Fe Kα come from the $(2.35\times)$ σ values given in Table 1. They were derived from the broad line fits to the spectra (see Table 1 references). They were usually estimated by fitting the X-ray continuum with (a) a nonthermal power-law, (b) a soft X-ray absorption law and (c) a hard reflection component. In general inclusion of component (c) enhances the continuum underlying the line resulting in a reduction of the derived EW and FWHM values. In some cases plausible solutions can cause the line to become unresolved (e.g. MCG-02-58-22).

Figure 2 shows that Fe Kα line is systematically broader than Hα in all *radio-quiet* AGN. In the case of MCG-6-30-15 (dots in Figure 6) and NGC 4151, FWHM(Kα)/FWHM(Hα) $\approx$ 40 and 10 respectively. The limited data for radio-loud sources shows a smaller difference in FWHM. For the Seyfert 1 galaxies listed in Table 3 we find: (1) the hypothesis that Fe Kα and Hα FWHM come from the same distribution is rejected at a confidence level $\gtrsim$ 0.995 using generalized (including upper limits for Fe Kα) Wilcoxon tests and (2) Fe Kα and Hα FWHM are not significantly correlated. A Kendall test with the inclusion of censored data yields a probability P$\approx$ 60% that a correlation is absent. EW values of Fe Kα and HI Hα are also not significantly correlated. The Spearman correlation coefficient is $r_S \approx 0.31$. For 25 data points the probability to have this value in a random sample of observations taken from an uncorrelated parent populations is 12 %. Restricting attention to the objects studied by Nandra et al. (1997), we do not find any significant correlation for half maximum centroid shifts. The most interesting trend emerging from a lineshift comparison is that the objects with a strongly redshifted broad component in Fe Kα show symmetric (unshifted) and relatively narrow HI Hα line profiles.

2.3. Possible Sources of Fe Kα Line Emission

Our considerations of origins for Fe Kα are focused on the Seyfert galaxies where the bulk of the Fe Kα spectral detections of reasonable S/N are found. In a unification driven approach we assume that: (1) a supermassive black hole and associated accretion disk lie at the center of each AGN, (2) Seyfert 2 galaxies (at least some of them) are Seyfert 1's seen edge-on (i $\gtrsim 45°$) and (3) the optical broad line emission region in Seyfert 2's is obscured by the putative cold dust torus. In this framework we can identify at least six possible origins for Fe Kα line emission (listed roughly in order of decreasing distance from the black hole): (A) cold Fe Kα emission from the obscuring dust torus which is assumed to be optically thin at $\sim$ 6keV in most cases (see e.g. Mushotzky et al. 1993: Ghisellini, Haardt & Matt 1994; Weaver et al. 1996); (B) Fe Kα emission from the classical BLR; (C) Fe Kα emission from a photoionized scattering region (a warm absorber); (D) cold Fe Kα emission due to fluorescence reflection (or emission) from the accretion disk; (E) Fe Kα emission from highly ionized coronal gas. Coronal gas (T $\gtrsim 10^9$ K) can give rise to strong Fe Kα emission at 6.67 or 6.97 KeV; (F) cold Fe Kα emission from a (non-disk) cloud distribution (not necessarily responsible for optical/UV LIL and/or HIL). Option (A), (B), (C), and (E) are briefly discussed below, as they appear rather unlikely to be the dominant source of Fe Kα emission. Option (D) and (F) deserve a much deeper discussion, deferred to § 3 and § 4 respectively. Our model considerations focus on MCG-6-30-15 as the best studied source with a characteristic broad Fe Kα line profile. The broadband spectrum of MGC-6-30-15 is consistent with a typical AGN continuum as described by Mathews & Ferland (1987; MF87) except that the sub-millimeter break may occur at higher energy than implied by their continuum ($\lesssim 1\times10^{-3}$ Ryd in MCG-6-30-15). We nonetheless assume that the sub-millimeter break occurrs at 1×10^{-5} Ryd as parameterized by MF87. The ionizing luminosity of MCG -6-30-15 is $L_{ion} \approx 6 \times 10^{43}$ ergs s^{-1} from $\log \nu L(\nu) \approx 29.0$ ergs s^{-1} at $\nu \approx 14$ Hz ($H_0 = 75$km s^{-1} Mpc^{-1}, and $q_0 = 0$ is assumed throught the paper; the corrected heliocentric radial velocity of MCG-06-30-15 measured on our spectrum is $v_{r,h} \approx 2317$ km s^{-1}, which implies a distance ≈ 30.9 Mpc.)

Table 4 reports expected line luminosities of MGC -6-30-15 for cases A, B. C, E. In Column (2) we report the Fe Kα luminosity computed in the case of gas with solar chemical abundances, while in Column (3) we report the Fe Kα luminosity in the case of a factor 10 iron overabundance with respect to the solar value. In Column (4) the dominant ionization stage of iron is reported. Column (5) lists the expected HI Hα luminosity. Luminosities are in ergs s^{-1}. These values should be compared to an observed total Fe Kα luminosity $\log L$(Fe Kα) ≈ 41.2, and to $\log L$(HI Hα) ≈ 40.8 . The L(Hα) value has been corrected for galactic extinction assuming $A_B \approx 0.15$, but not for internal absorption. The Fe Kα narrow component luminosity is $\approx$ 0.3–0.5 of the total L(Fe Kα).

2.3.1. Emission from a Dusty Torus

Option A would only give rise to a narrow Fe Kα line centered near rest energy. Strong variations observed in the "narrow" 6.4 keV part of the MCG-6-30-15 spectrum complicate this interpretation (Iwasawa et al. 1996b). For MCG-6-30-15 there is also a photon deficit problem. Table 4 reports the results of explorative `CLOUDY` (Ferland 1996) photoionization computations. A simple, optically thin model of a dusty torus, located between 3 and 10 pc, and photoionized by the central continuum source, produces a Fe Kα luminosity that is more than a factor ~ 100 below the observed Fe Kα luminosity. This remains true even if the attempt to ascribe to torus emission the "narrow component" only of the Fe Kα line. The situation may be markedly different in Sy 2 galaxies, where a narrow Fe Kα line is observed against a strongly absorbed X-ray continuum (Weaver et al. 1996; Ghisellini, Haardt, & Matt, 1994; Krolik, Madau & Życki 1994).

2.3.2. Warm Absorber

The warm absorber (option B) is also unlikely to be the dominant source of Fe Kα line emission (Reynolds & Fabian 1995; see Table 4). The photoionization calculations presented here are based on the model by Reynolds & Fabian: gas with T$\approx 10^5$K, $n_e \sim 10^6$ cm^{-3}, and moderate column density $N_c \sim 10^{22}$cm^{-2}, located within the BLR or at the outer edge of the BLR is photoionized by the AGN continuum. This model is not the only one proposed for the warm absorber (e. g., Mathur, et al. 1994), but it is probably adequate for low luminosity radio-quiet AGN. There are two main obstacles to "warm iron" Fe Kα emission. (a) a photon deficit; (b) the effects of Compton scattering on the line profile (Fabian et al. 1995). As a central corona is likely to be Compton thick, extreme broadening may occur (~ 1 keV; Fabian et al. 1995; Nandra et al. 1996).

2.3.3. Classical BLR

The main problem with Fe Kα BLR emission are that (1) there is a flux deficit, unless high iron abundances are invoked (see Table 4), and (2) Fe Kα and Balmer line width are inconsistent at least in Seyfert 1 galaxies (§ 2.2). Both problems are solvable if only the narrow component of the Fe Kα line is ascribed to the BLR. Our photoionization simulations show that, if iron abundance is 10 times the solar value, then the luminosity of Fe Kα produced within the BLR agrees with the observed luminosity of the Fe Kα narrow component.

The so called "X-ray Baldwin effect" (anticorrelation between Fe Kα EW and X-ray luminosity) has been interpreted as evidence for a common origin of Fe Kα and CIVλ1549 emission in the BLR (Iwasawa & Taniguchi 1993). The ASCA data do not support such an anticorrelation. The EW of Kα is strongly dependent on the fit of the X-ray continuum. If we consider the Iwasawa & Taniguchi (1993) objects for which ASCA observations are available (16 AGN, mainly low-luminosity), and that were fitted with a reflection component whenever appropriate, we find that the anticorrelation disappears (a Kendall's τ, generalized for the inclusion of censored data, yields $\approx$ 15 % probability of no correlation). We must point out, however, that if we substitute the ASCA data, and keep the other Iwasawa & Taniguchi (1993) values (a total of 38 objects), obtained from GINGA observations, then the correlation does not go away (Kendall's $\tau \Rightarrow$ P $\approx$ 0.003–0.007). As the resolution of the GINGA data was substantially lower, and the typical profile in Sy 1 galaxies resembles the one observed in MCG -06-30-15, with a broad redshifted component and a narrower component at 6.4 keV, a significant part of the broad companent may have been lost in the fit of the underlying continuum. The apparent lack of any "X-Ray Baldwin effect" in the ASCA data is therefore consistent with the idea that the Fe Kα narrow component only is emitted within the BLR (Marziani, et al. in preparation).

2.3.4. Hot Corona

A contribution from "hot iron" (more than 17 times ionized) cannot be ruled out for Seyfert nuclei because a high energy residual is observed for most Fe Kα disk candidates (see discussion in Section 4). We will show that, in fact, hot iron emission is expected from a photoionized disk. However, the most robust result of ASCA observations is that hot gas cannot be the dominant source of Fe Kα emission in Sy 1 galaxies, as the line energy is almost always around 6.4 keV, implying low ionization for iron (Nandra et al. 1997a). Nevertheless, coronal gas at a temperature close to the virial temperature $T_{vir} \approx 5 \times 10^{11}$ M_8 r_{14}^{-1} K, within r $\lesssim$ 10 –100R_g (where the gravitational radius $R_g = GM/c^2$) should be a strong Fe Kα emitter. The resulting Fe Kα luminosity is strongly dependent on the amount of matter that makes up such a corona. In Table 4, we compute a model assuming T=10^9K, and $N_c \approx 10^{25}$cm^{-2}. Redshifted hot coronal gas in addition to BLR emission provides an alternative to accretion disk emission. The observed profile may be reproduced equally well. The combined effects of gravitational redshift and increasing rest energy can produce centroid values $\gtrsim$ 5.0 at 6 R_g (6.19 keV at 20 R_g) if the ionization stage of iron is high. However, this requires some sort of fine tuning.

3. Broad Fe Kα and HI Hα Accretion Disk Models

Two independent lines of recent work consider emission from an accretion disk for Fe Kα (Życki & Czerny 1994; Matt, Perola & Stella 1992; Fabian et al. 1995; Dabrowski et al. 1997) and for HI Hα (Dumont & Collin-Souffrin 1990a,b & Collin-Souffrin & Dumont 1990; Rokaki, Collin-Souffrin & Magnan 1993, Eracleous & Halpern 1994). The first order fits to the Fe Kα line are qualitatively more satisfactory than fits to optical profiles. Model profiles computed for a rotating disk surrounding a Schwarzschild or Kerr black hole are most clearly consistent with the Fe Kα line profile observed in MCG-6-30-15 (dashed profile in Figure 6 shows Tanaka et al (1995) fit). However, as the number of Fe Kα detections increase, and line variability measures become more accurate, the disquieting trend is that model fits become poorer and require an ever larger range in the parameter space for disk models (e.g. Iwasawa et al. 1996b; Weaver et al. 1997). There is no evidence for convergence toward some characteristic disk model. Only a few other sources (Fairall 9, NGC4151, NGC5548, IC4329A) show structure unambiguously similar to MCG-6-30-15. This may be due to real profile differences or to the large variations in S/N of the data. The latter possibility is likely because the composite profile constructed by Nandra et al. (1997) from about 16 objects (see solid curve in Figure 6) is qualitatively similar to the MCG-6-30-15 profile. To summarize, one can fit almost any Fe Kα line profile with a disk model especially: (a) when one fits low S/N X-ray line profiles to models where most of the emission is produced at the innermost disk radii and (b) when the entire parameter space of Schwarzschild and Kerr models is available. Coupling this with assumptions about an emissivity law allows one to fit a disk model to any profile. This implies that a greater degree of self consistency is needed.

In the optical, where the lines are better defined the problems are basically the same, with the additional difficulty of *very* poor agreement between models and observations. Objects like Arp102B are rare–forcing disk emission advocates to argue that (1) objects with similar double-peaked profiles are most often obscured, and/or (2) that most emitters produce the line at larger radii in the disk (making the discovery of Arp102B somewhat miraculous). Truncation of line emission at r $\approx$ 1000 R_g demands a physical motivation that has yet to be found (see Eracleous & Halpern 1994).

Nonetheless, an accretion disk origin for the Fe line emission might offer a straightforward explanation for some important observational findings. If Fe Kα is emitted extremely close to the central black hole then that line emission is most sensitive to disk structure. This might explain why a number of intermediate redshift (z $\sim$ 1) quasars show neither strong Fe Kα nor a strong reflection continuum component (Nandra et al. 1997c). Disk structure could be markedly different in radio loud AGN as well. The standard α–disk

theory suggests that the region dominated by radiation pressure may not exist if the dimensionless accretion rate $\dot{m} \lesssim 0.4$ (Shakura & Sunyaev 1973; Frank, King, & Raine 1992). This case corresponds to the lowest luminosity AGN, which are thought to radiate in the sub-Eddington regime. In intermediate redshift quasars, the dimensionless accretion rate may approach unity, invalidating the thin disk assumption, and the central regions of the disk may puff up (Abramowicz, Calvani, & Nobili 1980; see also Calvani, Marziani, & Padovani 1989 for a review). In this case, we expect that Fe Kα is emitted only in the narrow funnel of the inflated disk, as its external layers would become too cool (Madau 1988). This would explain the rare detections of Fe Kα in intermediate and high redshift quasars, including both the radio-loud and radio-quiet variety, and observed dependence on luminosity of the line profile (Nandra et al. 1996; Nandra et al. 1997c). If Fe Kα is emitted in the funnel, then it can only be seen if the disk is observed nearly face-on, the rarest of the occurrences. It is intriguing that the only quasar where strong Fe Kα is detected, PG 1116+215 (Nandra et al. 1996), fits very well with this scenario. Model fitting of Fe Kα suggests i $\approx 0°$. The very narrow HI Hα profile, and the extremely strong $\mathrm{FeII_{opt}}$ emission make it a close replica of I Zw 1. These features can be explained in terms of emission from a face-on disk (Marziani et al. 1996).

LIL, HIL and Fe Kα might all arise from the same component with X-ray, UV and optical line emissivities peaking at different radii from the central continuum source. The FWHM difference described in § 2.3 could be accounted for if the X-ray lines were produced in a disk with Fe Kα produced near the center and the Balmer lines further out. At first glance the lack of a correlation between Fe Kα and Hα FWHM appears to pose a problem for models of this kind. This is not necessarily the case however because in disk models the width of Hα (FWHM) is driven by illuminating flux while FWHM Fe Kα is sensitively driven by the inner disk emitting radius.

3.1. A Disk Illumination Model for Both Hα and Fe Kα

In MCG -06-30-15, the Eddington ratio is $\eta_{\mathrm{Edd}} = \mathrm{L_{bol}/L_{Edd}} \lesssim 0.34$ ($\dot{\mathrm{M}} \approx 2 \times 10^{23}$ g $\mathrm{s^{-1}}$), consistent with the assumption of a thin disk down to the innermost stable orbit. We estimate a lower limit to the mass of the central black hole $\mathrm{M_{BH}} \gtrsim 4 \times 10^6 M_\odot$ from the assumption of cloud virial motion, following Padovani (1989). We assume $\mathrm{M}=10^7 \mathrm{M}_\odot$ and $\dot{\mathrm{M}} \approx 2 \times 10^{23}$ g $\mathrm{s^{-1}}$ in the computation of the disk structure (if line emission takes place in a disk the mass estimate should be divided by $\sin(< \mathrm{i} >) \approx 0.5$). We assume that this is appropriate for MCG-6-30-15 and all low-luminosity Seyfert 1's studied in this work.

We model the region where the continuum is produced as a sphere of radius r ≈ 100 $\mathrm{R_g}$

with $\tau_{es} \approx 0.25$. Radiation emitted in this region directly illuminates the disk, and is also partly scattered towards the disk by the free electrons in the sphere. In addition, a spherical halo of free electrons may surround the disk, up to 10^6 R_g, again with $\tau_{es} \approx 0.25$. Given the large uncertainty in the ionizing luminosity of AGN, we compute models for two extreme choices of the continuum: (a) the observed continuum, according to MF87. This choice probably overestimates the ionizing luminosity, as it includes the big blue bump and the reflection component that are thought to be produced within the disk; (b) a broken power law with slope -1.4 between 1×10^{15} Hz and 50 keV, and -2.5 for energy $\gtrsim$ 50 keV, which may yield an underestimate of the ionizing photon flux. Computation of the scattered flux as a function of disk radius is as carried out by Rokaki et al. (1993). Relativistic effects (most notably returning radiation i. e., radiation emitted by an accretion disk which returns to its surface due to gravitational focusing or the shape of the disk; Cunningham 1976) are neglected in the scattering process, even if they are thought to be relevant in the innermost region of the disk. Returning radiation may enhance Fe Kα emission by a factor ≈ 2 (Martocchia & Matt 1996; see also Dabrowski et al. 1997).

We consider here the radial disk structure appropriate for a Kerr metric, with the angular momentum per unit mass a = 0.998 M (c = G = 1; as shown by Thorne 1974, the radiation emitted by the disk and swallowed by the hole prevents spin up beyond a limiting state $a/M_{lim} \approx 0.998$ M; the corresponding innermost stable orbit is at r$\approx$ 1.25 R_g) and use the equations for the radial and vertical structure of a standard α-disk model, with the corrective terms given by Novikov and Thorne (1973). The disk is divided into concentric annuli of fixed fractional width $\Delta r/r \approx 0.2$. Surface density, column density, and illuminating flux are assumed constant within each annulus. We approximate the hydrostatic equilibrium (leaving the vertical structure unperturbed by the incoming radiation) assuming that the density within the disk increases linearly with column density. This is a crude approximation since the vertical structure of the disk should be recomputed to take into account the heating provided by the illuminating flux. In the outer layers of the innermost regions, if the density is too low and the radiation density too high (for values of $\xi = L_{ion}/r^2 n_e \sim 10^4$ ergs s^{-1}cm), the gas is heated to $T \sim 1 \times 10^{10}$ K. In this case the disk layer actually becomes part of a corona, and we assume that radiation penetrates to a layer within the disk of optical depth larger by $\Delta\tau_{disk} = 1$, with flux reduced by a factor $\exp(-\Delta\tau_{disk})$. We employed the photoionization code `CLOUDY` (Ferland 1996) to compute the emissivity in the Fe Kα and Balmer lines.

3.2. Illumination Model Results

3.2.1. Fe Kα

We identify four vertical zones within the disk. (a) Very hot gas – a halo that has undergone a thermal runaway due to heating by scattered radiation in the lowest density layers of the disk ($\tau < 1$). (b) Warm gas in an "intermediate" region of higher density, whose electron temperature varies from $\gtrsim 10^7$ down to a few 10^4 K. (c) Ionized gas at a few 10^4 K; (d) cold, almost neutral gas which is less heated by the incoming radiation (T $\lesssim$ few $\times$ 10^3 K). Reflection models usually suggest that the "cold" Fe Kα emission is produced in the two deepest layer. In Table 5 we report the results of our calculations. In Column (1) we give an identification number for each model. In Columns (2) (3), (4), (5) the inner and outer radii, and the electron scattering optical depth for the inner sphere and the outer halo are reported. In Column (6) we list the shape of the continuum (as described in the previous section). Column (7), (8), and (9) yield the logarithms of the Fe Kα luminosity from cold iron emission, the ratio L(Fe Kα)$_{\rm Hot}$/L(Fe Kα)$_{\rm Cold}$, and the log(L(Hi Hα)) respectively.

Our model of the vertical disk structure allows us only a coarse estimate of the relative flux contributions from "cold" and "hot" iron. The computed ratio Fe$_{\rm Hot}$/Fe$_{\rm Cold}$ ($\approx 0.1 - 0.3$) is sensitive to returning radiation which is not taken into account. The predictions of our model for Fe$_{\rm Hot}$/Fe$_{\rm Cold}$ are nevertheless in qualitative agreements with those of Matt, Fabian & Ross (1996). We are also aware that mean escape probability formalisms are not adequate for the treatment of Compton scattering and radiative transfer of the Fe Kα line. Nevertheless, our photoionization calculations for cold Fe Kα agree with the results of Monte Carlo simulations of Fe Kα emission from a homogeneous layer of cold matter by George & Fabian (1991). They find that $\approx 6\%$ of the photons between 9 and 30 keV are converted into Fe Kα photons. This yields L(Kα) $\approx 1.2 \times 10^{41}$ ergs s^{-1} for MCG-6-30-15 (the observed total Fe Kα luminosity is L(Fe Kα) $\approx 1.6 \times 10^{41}$ ergs s^{-1}).

From Table 5 we deduce also that the observed luminosity values for MCG -6-30-15 are in the range predicted by our disk models. We must remark that the choices of the continuum are probably extreme (new observations suggest that the "big blue bump" may not be as prominent as previously thought; Laor et al. 1997). The MF87 continuum gives rise to line luminosities somewhat larger than observed, as the observed L(Kα) of MCG -6-30-15 in the "medium phase" is $\approx 1.6 \times 10^{41}$ ergs s^{-1} (Isawasa et al., 1996). On the other hand, the "power-law" continuum has an ionizing luminosity a factor ~ 10 lower than that of the MF continuum, for the same optical flux, and it therefore not surprising that fluxes are lower than observed. The total Hα luminosity is rather sensitive to the presence of an outer halo, but the Fe Kα luminosity is not, as emission in the innermost disk region $\lesssim$ 20 R$_{\rm g}$ is by far the strongest. Figure 3 shows emissivity profiles for Hi Hα and Fe Kα

derived from our models.

Next we computed the cold Fe Kα line profile following Fanton et al. (1997), and using the emissivity law obtained from Model 1. The code developed by Fanton et al. computes the trajectories in the full Kerr metric taking into account all the relevant general relativistic effects. The computed profile is therefore accurate at any distance beyond the event horizon and for disks seen at any inclinations. Integration was carried out in between 1.25 $R_g \lesssim r \lesssim 20\ R_g$. Figure 4 shows the results of our fits to the MCG-6-30-15 data (Tanaka et al. 1995) where we were able to satisfactorily reproduce the Fe Kα profile.

3.2.2. HI Hα

The vertical stratification of density implies a variety of physical conditions within the disk. This has the important implication that the disk is able to produce Balmer line emission at almost any distance from the continuum source, in regions (c) and (d) of §3.2.1. The Hα emissivity law for Model 1 can be approximated with a shallow power law ($p = -0.71$) for $10^2\ R_g \lesssim r \lesssim 10^4\ R_g$ and with a steeper law ($p=-2.33$) for $r \gtrsim 10^6\ R_g$. This emissivity law makes the production of symmetric single-peaked profiles very likely, as the emissivity favors emission from the outer regions of the disk, where relativistic effects are negligible. $\epsilon(r) \times r^2$ peaks at $r \sim 10^4\ R_g$, a value that is in agreement with the average distance for Balmer line emission deduced from reverberation mapping. Fig. 5 shows superimposed Hα and disk profiles based on model 1 for 15 Seyfert 1's included in the Nandra et al. (1997a) sample. Model profiles were computed following Chen & Halpern (1989) rather than Fanton et al. (with the emissivity law of Model 1) as their weak field approximation is adequate for the relativistic treatment at large radii. Best fits were achieved using the downhill simplex algorithm by Nelder & Mead (1978). The outer radius of the emitting region was allowed to vary within a narrow range, $10^5\ R_g \lesssim r_{out} \lesssim 10^6\ R_g$ (the distance at which disk fragmentation due to self gravity is expected to become relevant). An additional free parameter is a scale factor. In Table 6 we report the results of HI Hα disk model fitting. The format is: Column 1 and 2 - IAU code and common name; Column 3 - r_{out}; Column 4 - HI Hα disk inclination from our model 1 fits; Column 5 - the reduced χ^2; Column 8 - Column 6 and 7 inclination and reduced χ^2 for Model 2 fits (not shown in Fig. 5); Fe Kα disk inclination from Kerr model fits (Nandra et al. 1997). Hα model fits of 3C 120. Statistically good fits are the ones with $\chi^2 \lesssim 1$. The formal uncertainty in the estimate of the inclination is typically a few degrees (it is undefined if the fit is not statistically good), but the actual uncertainty is probably much larger. The distribution of scattering matter affects the estimate of the inclination, since it change the

turning point in the slope of the emissivity laws (Fig. 4). Model 1 and Model 2 should be regarded as limiting cases for the emissivity law.

3.2.3. Main Results and Implications

Our attempt to constrain the disk models has met with mixed success. We summarize here the main achievements and problems.

- There is poor agreement between the disk inclination derived from X-ray and optical lines for MCG-6-30-15. This is an especially disturbing case. The extremely narrow HI Hα profile requires small inclination while the broad FE Kα profile constrains it to $\approx 30^{\circ}$, even in the case of a Kerr black hole with a$\approx$M. Disk inclination is the only free parameter for our model because the inner and outer emitting radii are constrained by the emissivity law. ~ 7 objects studied by Nandra et al. (1997a,b) have derived Kα disk model inclinations well enough constrained for comparison. The small number precludes a reliable statistical analysis. Even including some objects with uncontrained inclination from FE Kα data, we find a statistically good fit for HI Hα and inclination consistency between HI Hα and FE Kα only for NGC 3227, NGC 3783, Mark 841, NGC 4593, NGC 7469 and NGC 5548.

- Disk models do not reproduce most Balmer line profiles of Seyfert galaxies. This is most likely true for all models computed in this paper. There is no known physical reason to limit the emitting radius of HI Hα except for the outer radius at which the disk fragments (10^5 - 10^6 R_g). Integrating within this limit, line cores are well reproduced only when they are symmetric and unshifted. The shape and asymmetry of line wings also does not agree with disk model predictions (Romano et al. 1996).

- The comparison between observed and disk model HI Hα profiles suggests a simple variant of the old cloud model (see e.g. Mathews & Capriotti 1985, and references therein) capable of explaining the new data: a flattened ensemble of dense ($n_e \sim 10^{10}$ to $\sim 10^{13}$cm^{-3}) clouds, co-axial with the accretion disk, spiralling inward (or outward) because of drag forces, on a time-scale much shorter than the radial drift time scale for an α-disk. Cloud production might occur in a wind from the disk surface, or the wind itself could be a source of HI Hα and CIVλ1549 line emission (e. g., Murray & Chiang 1997).

  The real challenge for any BLR model is not the ability to reproduce one single profile, but rather to account for the distribution of line width, shift and asymmetry

observed in any sample of AGN. No model proposed until now has achieved this goal. Asymmetries may be produced because the clouds are optically thick to the lines they emit (i.e. the lines we observe come mostly from the illuminated face of the cloud), and because of the spiralling path. If the system of clouds is observed nearly face on, then we have symmetric, unshifted, profiles, and the narrowest of all observed profiles. Larger asymmetries are expected if the line is broader (as observed): in this case line emitting clouds have a larger component of their non-circular velocity along the line of sight.

- The Fe profile shape may be complicated by a significant and variable contribution from hot Fe. This may help account for the large observed EW's and provides an additional free parameter for adjustment to the profile shape. In particular it might account for the wing on the high energy side of the line observed in sources like MCG-5-23-16 (Weaver et al. 1997).

4. Other Models for Fe Kα Emission

4.1. Major Challenges for Disk Models

An important uncertainty, that affects our interpretation of the Fe line origin, is whether it arises from a single emitting region. Almost all past disk model fits, including the previous section, have treated the Fe Kα line as a single component. There are several forms of evidence to support the hypothesis that the line is composite.

1) Many Seyfert 1 spectra show a narrow Fe Kα peak very close to the rest energy of 6.4 keV. This is not a problem for a wide range of disk models and is, in fact, consistent with the expectation of a Doppler-boosted blue peak from an illuminated disk viewed at intermediate inclination. The fact that the blue peak always occurs at 6.4 keV would just be a coincidence. However the narrow feature can also be reasonably ascribed to an unshifted independent component. This possibility is strengthened because some of the best line profiles, including MCG-6-30-15, show a smooth high energy (blue) wing. Nandra et al. (1997) present composite spectra (see solid curve in Figure 6) made both with and without the two "best" examples, MCG-6-30-15 and NGC 4151. Both composite spectra show a similar blue wing on Fe Kα suggesting that it is a common property of Seyfert 1 line profiles. The range of disk models explored in the literature almost always show a sharp drop on the blue side of the profile which is inconsistent with this blue shoulder. The recent detection of MCG-5-23-16 (Weaver et al. 1997 - not included in the Nandra et al. 1997 study), exacerbates this problem showing perhaps the strongest blue shoulder yet observed.

An obvious decomposition of the line into two symmetric Gaussian components is: (1) a narrow component centered at E_n=6.4±0.05 keV with FWHM=0.25 keV and (2) a broad component centered at E_b=5.9±0.1 keV with FWHM=1.6 keV. The blue wing appears to be a natural extension of the second component under the first rather than an independent feature.

2) Recent variability results for the best studied Seyfert 1 MCG-6-30-15 show that the narrow "blue" (6.4keV) and broad red components vary independently (Iwasawa et al. 1996b). The blue peak responds quickly to continuum changes while the red peak responds more slowly or remains relatively constant. This is again consistent with the notion that we are observing two independent features. The variability studies add another problem for disk models. Pre-ASCA variability studies (Mushotzky et al. 1993) already found potential problems with disk models because the Fe Kα line did not show the relatively short time scale response to continuum changes that is expected from simple disk models. This issue is discussed in a companion paper (Sulentic et al. 1997).

3) Many objects show breaks in the red wing that could indicate discrete components. Only higher s/n observations will decide if the red wing is continuous and consistent, in detail, with disk models. The recent Fe Kα detection in MCG-5-23-16 shows clear evidence for two or three components (one at 6.4 keV as discussed above) (Weaver et al. 1997). Model fits to the broad feature in MCG-5-23-16 leave a significant residual between 5-6 keV and possibly also on the blue side. A 5.5 keV component was also discussed for NGC 4051 (Guainazzi et al. 1996) and 3C 109 (Allen et al. 1997) however the latter reference suggests that this may be related to an instrumental artifact.

4) Finally there is the problem raised by unification models that view (at least some) Seyfert 2 galaxies as edge-on Seyfert 1's where the BLR is obscured by a dust torus (see also Turner et al. 1997 and Nandra et al. 1997). Seyfert 2 galaxies are most probably an heterogeneous class, but there is evidence that Seyfert 2 with Fe Kα detections may be genuinely obscured Seyfert 1 (see e. g., Dultzin Hacyan 1997, and private communication). Emission from an inclined disk would produce broad profile which are easily distinguishable. Only Seyfert 2 sources IRAS 18325-5926 and MCG-5-23-16 can be reasonably well fit with disk models. The red asymmetry and blue-shifted blue peak are consistent with a reasonably high inclination (i=40-50°: Iwasawa et al. 1996a) as expected for a Seyfert 2. The current status of disk emission models for Fe Kα lines in Seyfert 2 objects hearkens back to the situation for a disk signature in optical broad lines as discussed in the introduction. If we see an obvious disk signature in IRAS18325-5926 (and MCG-5-23-16) then where is the corresponding signature in other Seyfert 2 objects? Why we do not see an edge-on disk profile in NGC 1068 (this object may be optically thick out to 20 keV: Mushotzky et

al. 1993), NGC 3147 and 6552 as well as Markarian 3 and other Seyferts 2's observed by ASCA? The lack of coherence in the model fits to different AGNs of the same subclass is already disturbing. The large equivalent width of the IRAS18325-5926 detection (and now also MCG-5-23-16), if from a disk, suggests that many other inclined (but not edge-on) disks should be detectable.

4.2. Alternatives to Fe Kα Disk Emission

Alternative models for the complex emission profile near 6.4 keV (or just the broad component) must avoid the difficulties that were summarized in the preceding section. They must also satisfy the following general requirements: (a) produce strong Fe Kα emission (EW$\sim$100-200eV), (b) broaden it (σ $\sim$0.6keV), (c) red shift the bulk of the emission and (d) to a lesser extent, symmetrize the line (assuming that the narrow and broad components are independent). It must also account for the FWHM difference between Fe Kα and the UV/optical HIL/LIL if a BLR unification is attempted. The first task can be accomplished with an ensemble of emitting clouds provided that the column density is high enough and the covering factor is in the range 55-85% (Sivron and Tsuruta 1993; Nandra & George 1994). The strength of the line is a problem for disk and non disk models alike. A photoionized medium is one of the solutions previously proposed for this problem (e.g. Tanaka et al. 1995). The line profile can be broadened most easily by increasing the velocity dispersion of the cloud ensemble but possible constraints imposed by the sharpness of absorption edges (Fabian et al. 1995) motivate us to look for solutions that minimize Doppler broadening. Several other possibilities have been considered, some of which could also introduce the required red displacement that is observed (e.g. Fabian et al. 1995) by (1) Comptonization, (2) transverse Doppler effect and (3) gravitational redshift.

The difference in average profile FWHM between Fe Kα and Hi Hα greatly constrains non-disk models where Fe Kα arises in the optical broad line clouds. Our previous work on modeling optical line profiles with bi-conical emission structures (as alternatives to disk models; Zheng, Binette, & Sulentic 1990) leads us to consider that possibility also for Fe emission. A bi-cone model might provide an explanation for the strong changes observed in the narrow component of MCG-6-30-15. As the approaching side of the bi-cone should be the one closest to the observer, one could see variations following continuum variability with essentially zero time delay. This is especially true if the opening angle of the cone is small. Dense clouds ($n_e \gtrsim 10^{13}cm^{-3}$ are a likely producer of Fe Kα, and a continuum reprocessor as well (Guilbert & Rees 1988; Lightman & White 1988) giving a flattening of the X-ray spectrum similar to the situation for a disk reflection component. Such dense

clouds should not be a strong source of Balmer line emission.

4.2.1. A First-Order Model

We made a first-order test of the possibility that the Fe Kα line emission is produced in a cloud ensemble surrounding the central source. Earlier work on a cloud model was discussed in the previous section. Our extension of this work is intended to show only that a biconical cloud distribution can reproduce the most complex Fe Kα line profiles. Options include modeling: (1) the entire Fe line profile for MCG-6-30-15, (2) the entire average profile (Nandra et al. 1997) and (3) the broad redshifted part of the average profile. The first two options are essentially equivalent so we focus on MCG-6-30-15 as an extreme example of option 2. This source has perhaps the best defined and most studied profile of any Sy I detection. Options 1 and 2 represent the greater challenges because it is certainly easier to reproduce a Gaussian profile with a cloud ensemble model.

We initially assume that the red component is produced by clouds at rest at a distance r moving at speed v from the central source. The gravitational redshift formula:

$$\lambda/\lambda' = [1 - (v/c)\cos\theta]/[\sqrt{(1 - v^2/c^2)(1 - 2GM/(c^2 r))}]$$

(where λ is the rest frame wavelength, λ' is the shifted wavelength, θ is the angle between the line of sight and the cloud velocity, M the mass of the central black hole) then allows us to convert the observed profile into an intensity distribution I(r) contributed by shells at various radii from the central source. In the case of the redshifted part of the average profile the emission peaks at r = 12 R_g with a sharp drop towards smaller radii and an I(r)$\propto$ r^{-1} tail in the opposite direction. The higher redshift of the MCG-6-30-15 profile implies even smaller distances from the central source. The bulk redshift of the line is a consequence of the fact that the majority of the emission arises very close to the black hole. This conclusion is true for any kinematical model, including emission from an accretion disk, and does not depend on the specific geometric assumptions.

Unfortunately it is hard to explain why the clouds at only a few gravitational radii from the black hole would be at rest. The gravitational potential is very steep and the radiation pressure is unlikely to be important because we are in the sub-Eddington regime. A marginally bound particle passes 10 R_g with a velocity of 0.45 c during radial infall. With motion being dynamically important one must make assumptions about the geometry and energetics. Our first-order model considers clouds with predominantly radial motion. Angular momentum tends to circularize any cloud distribution therefore making it impossible to explain the double peaked line profile observed in MCG-6-30-15 (unless a very

specific planar geometry is assumed as in the case of an accretion disk). We constructed models for both radial infall and outflow. As we show below inflow is clearly preferred by model fits to the observations. This is consistent with the arguments based on energetics. It seems very hard to accelerate the matter outwards in a region only a few R_g from the black hole.

The assumptions of the model are as follows: (i) Clouds are in radial bound orbits defined by their apastron distance R where the clouds would be at rest. The profile is reproduced from a Monte Carlo simulation of individual cloud contributions. The distribution of distances r of the clouds is calculated from the time *dt* clouds are spending between shells r and r + dr. (ii) The cloud distribution is limited by the inner radius r_{in} (we assume $r_{in} = 6\ R_g$) and the outer radius $r_{out} < R$ ($r_{out} = 15\ R_g$ was assumed throughout). (iii) The clouds are confined to double cones with a half-opening angle i_c. (iv) The inclination of the line of sight towards the cone axis is i. (v) Emission in the comoving frame of the cloud is isotropic in the optically thin case, and confined to the inward looking hemisphere for the case of optically thick Fe Kα emission (both cases are feasible, see Nandra and George 1994). The intensity of emission in the comoving frame does not depend on distance from the central source.

Cone models often suffer from a large number of assumptions involving geometry and emissivity laws. Our fitting is only illustrative so we do not pretend to explore the whole parameter space here. Instead, by using the model outlined above, we keep the number of parameters reasonably low: only the apastron distance and the inclination were fit, with the rest being assumed or of second order importance. This is similar to accretion disk models where the critical parameters are the inclination and the distance of its inner edge.

Figure 6 shows the results of our model fits. The thick histogram shows an example of the line profile we get for radial inflow of optically thin clouds and the thin histogram shows the optically thick counterpart. The inclination ($i = 20°$) is intermediate and the cone is wide ($i_c = 50°$). The value of apastron distance R is important. Here, as in all other attempts, we were forced to assume that the velocity of the clouds approaches zero at the outer edge of the cloud distribution which is still fairly close to the BH (this is consistent with the CLOUDY calculation presented above). Although on one hand a consequence of this assumption is that thesse clouds do not reach large distances from the central source that would blur the relatively sharp observed O VII edge attributed to the warm absorber (Fabian et al. 1994a, 1995), on the other hand it is difficult to explain why the velocity would not be higher, i.e. closer to that of marginally bound infalling clouds. The accretion disk scenario escapes extreme velocities by invoking nearly face-on orientation. In a bi-cone model such a projection effect seems unlikely unless an inclination nearly perpendicular to

the cone axis is assumed. In this case the contributions from both cones merge in a single Gaussian-like redshifted component. It is easy to fit the redshifted Gaussian component of the average profile this way, but not the well defined peak and red shoulder of the MCG-6-30-15 profile. We do not attempt to explain the low radial velocity of clouds at $\sim 15R_g$ here. Possible explanations include a contribution from an ion torus or from a geometrically thick inner edge of a surrounding accretion disk. Mathews (1993) was able to "bounce" clouds around an equilibrium radius (where gravity was balanced by radiation forces) about an order of magnitude larger than the one considered here.

It would be satisfying to fit the average profile using the same parameters as used for the MCG-6-30-15 fit, varying only the inclination to the line of sight. Unfortunately we can not envision a model where this is true, accretion disk models included. In the case of a bi-cone the higher inclination angle causes the peaks to merge so that the narrow component at the rest energy must have a separate origin (an interpretation that we favor). A convenient way to fit both components of the average profile with a single zone model would involve the assumption of varying optical thickness of the emitting clouds. The thin lined histogram in Fig 5 uses the same parameters as the MCG-6-30-15 fit, but assuming the optically thick regime. The low energy peak is weaker as a consequence of the fact that the optically thick inward moving clouds on our side of the BH emit most of light away from us, while we still see the bright faces of the clouds that lie on the other side and move toward us. The observed average profile lies between both histogram curves and therefore it is reasonable to conclude that the full range of observed Fe Kα lines can be explained by different optical thickness of the clouds (Nandra and George 1994).

The model outlined above allows us to distinguish between two kinds of radial motion, i.e. inflow and outflow. Some of the photons originating in the far-side cone are intercepted by the BH, so the contribution from the far-side cone is weaker. The blue part of the profile gets weaker if inflow is considered, while the red part is weaker in the case of outflow. In all of our Monte Carlo simulations it was hard to avoid too much flux in the high energy wing of the line. The contribution from clouds close to the black hole moving towards the observer was acceptably low only for the case of inflow (though the high energy flux is still higher than observed, cf. the thick histogram in Fig. 5). The distinction between both directions of motion is even more obvious in the explanation of the difference between the MCG-6-30-15 and the average profile as outlined above. If we deal with outflow it is the high energy peak that gets weaker when we switch from the optically thin to the thick regime, i.e. opposite to the case observed.

We conclude that a simple double cone model has the potential to explain both the MCG-6-30-15 and the average Fe Kα profile allowing only for a variation of optical

thickness of the emitting clouds. This can be further used to explain the observed variations in some objects. This is encouraging, still a physical explanation of the origin of low velocity clouds at $\sim 15 R_g$ is clearly needed but is beyond the scope of this paper.

5. Summary of Results & Implications for AGN Models

The main results of this investigation are as follows:

1. The bulk of Fe emission near 6.4 keV cannot be directly associated with the optical BLR. Fe Kα and HI Hα lines show significantly different width and are therefore not emitted in the same BLR region in radio-quiet objects, at least not at the same distance from the central continuum source.

2. A simple illumination model suggests that both Fe Kα and HI Hα could be emitted by an accretion disk, although the bulk emission for the two lines would arise at widely different radii (Fe Kα $\lesssim$ 100 R_g; HI H$\alpha \sim 10^3$ R_g).

3. While our illuminated disk model is able to predict HI Hα profile widths and emitting radii consistent with observational results, the observed and model profile shapes show poor agreement. The Fe Kα emission line data are also inconsistent with a single emissivity law. There is poor agreement between disk inclination values derived for Fe Kα and HI Hα. Observed HI Hα asymmetries and shifts demand a larger radial drift velocity than compatible with Keplerian disk models.

4. Evidence is accumulating to suggest that the Fe Kα line may be composed of (at least) two independent components. If the broad component is independent and also shows Gaussian symmetry as suggested by the Nandra et al. (1997b) composite spectrum, there are no obvious disk models consistent with it. Physically, there are viable alternatives. The narrow component could be due to BLR emission with a smaller contribution from the warm absorber, while the broad component could be redshifted coronal emission.

5. First-order models involving a biconical distribution of emitting clouds are able to reproduce the observed Fe Kα spectra for AGN. They can also easily account for the observations that raise serious problems for the disk emission scenario.

6. Acknowledgements

J. W. S. acknowledges support under NASA AR-05293.01-93A from STScI and Consiglio Nazionale per le Ricerche (CNR). P.M. acknowledges the hospitality of UNAM, University of Alabama and the Ljubljana University where parts of this work were done. We would like to thank an anonymous referee whose comments greatly improved the presentation of this paper.

7. References

Abramowicz, M., Calvani, M., and Nobili, M., 1980, ApJ, 242, 772

Allen, S., Fabian, A., Idesawa, E., Inoue, H., Kii, T. and Otani, C., 1997, MNRAS, 286, 765

Antonucci, R., and Miller, J. S., 1985, ApJ, 297, 621

Calvani, M., Marziani, P., and Padovani, P., 1989, in Proceedings of the VIII Italian Symposium on General Relativity and Gravitation. (Singapore: World Scientific Co.), 102

Cassidy I., and Raine, D. J., 1993, MNRAS, 260, 385

Chen, K., and Halpern, J. P., 1989, ApJ, 344, 115

Chen, K., Halpern, J. P. and Filippenko, A. V., 1989, ApJ, 339, 742

Collin-Souffrin, S. and Dumont, A. – M., 1986, A&A, 166, 13

Collin-Souffrin, S. and Dumont, A. – M., 1990, A&A, 229, 292

Cunningham, Chr., 1976, ApJ, 208, 534

Dabrowski, Y., Fabian, A. C., Iwasawa, K., Lasenby, A. N., & Reynolds, C. S., 1997, MNRAS, 288, L11

Done, C. et al. 1996, ApJ, 463, L63

Dumont, A. – M., and Collin-Souffrin, S., 1990a, A&AS, 83, 71

Dumont, A. – M., and Collin-Souffrin, S., 1990b, A&A, 229, 313

Dultzin-Hacyan, D., 1997, RMxAA Serie de Conferencias, 6, 132

Elvis, M. et al., 1994, ApJ, 436, L55

Eracleous, M., and Halpern, J. P., 1994, ApJS, 90, 1

Eracleous, M., et al., 1996, ApJ, 459, 89

Fabian et al., 1994a, PASJ, 46, L59

Fabian, A. et al., 1994b, ApJ, 436, L51

Fabian, A. C., Nandra, K., Reynolds, C. S., Brandt, W. N., Otani, C., & Tanaka, Y. 1995, MNRAS, 277, L11

Fanton, C., Calvani, M., de Felice, F., and Čadež, A. 1997, PASJ, 49, 159

Ferland, G. J., and Rees, M. J., 1988, ApJ, 332, 141

Ferland, G. J., 1996, Hazy: a brief introduction to CLOUDY, University of Kentucky, Dept. Phys. Astron., internal report

Filippenko, A. V., and Sargent, W. L. W., 1988, ApJ, 324, 134

Frank, J., King, R., and Raine, D., 1992, Accretion Power in Astrophysics (2nd edition), (Cambridge: Cambridge University Press)

Fukazawa, Y. et al., 1994, PASJ, 46, L141

Gaskell, C. M., 1982, ApJ, 263, 79

Gaskell, C. M., 1996, ApJ, 464, L107

George, I. M., & Fabian, A. C., 1991, MNRAS, 249, 352

George, I. et al., 1995, ApJ, 438, L67

Ghisellini, G., Haardt, F. and Matt, G., 1994, MNRAS, 267, 743

Gonzalez–Delgado, M., and Perez, E., 1996, MNRAS, 278, 737

Guainazzi, M., Matsuoka, M., Piro, L., Mihara, T., and Yamauchi,, M., 1994, ApJ, 436, L35

Guainazzi, M., Mihara, T., Otani, C., and Matsuota, M., 1996, PASJ, 48, 781

Guilbert, P. W., and Rees, M. J., 1988, MNRAS, 233, 475

Halpern, J., et al., 1997, ASCA Cherry Blossom Conference

Hayashi, I. et al., 1996, PASJ, 48, 219

Ho, L. C., Filippenko, A. V., and Sargent, W. L. W., 1995, ApJS, 98, 477

Ishisaki, Y., et al., 1996, PASJ, 48, 237

Iwasawa, K., and Taniguchi, Y, 1993, ApJ, 413, L15

Iwasawa, K., et al., 1994, PASJ, 46, L167

Iwasawa, K., et al., 1996a, MNRAS, 279, 837

Iwasawa, K., et al., 1996b, MNRAS, 282, 1038

Laor, A., Fiore, F., Elvis, M., Wilkes, B., & McDowell, J., 1997, ApJ, 477, 93

Lightman, A. P., & White, 1988, ApJ, 335, 57

Krolik, J. H., Madau, P., & Życki, P. T., 1994, ApJ, 420, L57

Madau, P., 1988, ApJ, 327, 116

Makishima, K. et al., 1994, PASJ, 46, L77

Martocchia, A., and Matt, G., 1996, MNRAS, 282, L53

Marziani, P., Calvani, M., and Sulentic, J. W., 1992, ApJ, 393, 658

Marziani, P., Sulentic, J. W., Dultzin-Hacyan,, D., Calvani, M., & Moles, M., 1996, ApJS, 104, 37

Mathews, W. G., 1993, ApJ, 412, L17

Mathews, W. and Ferland, G., 1987, ApJ, 323, 456 (MF87)

Mathews, W. G., & Capriotti, E. R., 1984, in Astrophysics of Active Galaxies and Quasi-stellar Objects, J. S. Miller (Ed.), (Mill Valley: University Science Books), p. 184

Matt, G., Perola, G. C. and Stella, L., 1992, A&A, 257, 63

Matt, G., Fabian, A. C., and Ross, R.R., 1996, MNRAS, 278, 111

Mihara, T. et al., 1994, PASJ, 46, L137

Morris, S. L., Ward, M. J., 1988, MNRAS, 230, 639

Morris, S. L., Ward, M. J., 1989, ApJ, 340, 713

Murray, N., & Chiang, J., 1997, ApJ, 474, 91

Mushotzky, R. F., 1997, RMxAC, 6, 213

Mushotzky, R. F., Done, C., and Pounds, K. A., 1993, ARA&A, 31, 717

Mushotzky, R. F., Fabian, A. C., Iwasawa, K., Kunieda, H., Matsuoka, M., Nandra, K., and Tanaka, Y., 1995, MNRAS, 272, L9

Nandra, K. and George, I., 1994, MNRAS, 267, 974

Nandra, K., George, I. M., Turner, T. J. and Fukazawa, Y., 1996, ApJ, 464, 165

Nandra, K., George, I. M., Mushotzky, R. F., Turner, T. J., & Yaqoob, 1997a, ApJ, 476, 70

Nandra, K., George, I. M., Mushotzky, R. F., Turner, T. J. and Yaqoob, T., 1997b, ApJ, 477, 602

Nandra, K., George, I. M., Mushotzky, R. F., Turner, T. J. and Yaqoob, T., 1997c, ApJ, 488, L91

Nelder, J. A., and Mead, R., 1965, Computer Journal, 7, 308

Novikov, I., and Thorne, K. S., 1973, In: Black Holes, Eds. De Witt, B. S. and De Witt, C., (Gordon & Breach: New York)

Osterbrock, D. E., and Pogge, R. W., 1985, ApJ, 297, 166

Osterbrock, D. E., and Shuder, J. M., 1982, ApJS, 49, 149

Padovani, P., 1989, A&A, 209, 27

Pounds, K., et al., MNRAS, 1994, 267, 193

Pounds, K. et al., 1995, MNRAS, 277, L5

Ptak, A. et al., 1994, ApJ, 436, L31

Ptak, A. et al., 1996, ApJ, 495, 542

Puchnarewicz, E. M., Mason, K. O., Siemiginowska, A., and Pounds, K. A., 1995, MNRAS, 276, 20

Rafanelli, P., and Schulz, H., 1983, A&A, 117, 109

Reynolds, C., 1997, MNRAS, 286, 513

Reynolds, C. S., and Fabian, A. C., 1995, MNRAS, 273, 1167

Reynolds, C. S. et al., 1995, MNRAS, 276, 1311

Rokaki, E., Collin-Souffrin, S., and Magnan, C., 1993, A&A, 272, 8

Romano, P., Zwitter, T., Calvani, M., Sulentic J. W., 1996, MNRAS, 279, 165

Shakura, S., & Sunyaev, R., 1973, A&A, 24, 337

Shuder, J. M., 1981, AJ, 86, 1595

Sivron, R. and Tsuruta, S., 1993, ApJ, 402, 420

Smith, D. and Done, C., 1996, MNRAS, 280, 355

Sulentic, J. W., 1989, ApJ, 343, 54

Sulentic, J. W., Calvani, M., Marziani, P., & Zheng, W., 1990, ApJ, 355, L15

Sulentic, J. W., Marziani, P., Zwitter, T. and Calvani, M. 1995a, ApJ, 438, L1

Sulentic, J. W., Marziani, P., Dultzin-Hacyan, D., Calvani, M, and Moles, M., 1995b, ApJ, 445, L85

Tanaka, Y., Holt, S. S., and Inoue, H., 1994, PASJ, 46, L37

Tanaka, Y., et al., 1995, Nature, 375, 659

Thorne, K., 1974, ApJ, 191, 507

Turner, T. J., et al., 1996, ApJ, 463, 134

Turner, T. J. George, I. M., Nandra, K., Mushotzky, R. F., 1997, ApJ, 488, 164

Ueno, S. et al., 1994, PASJ, 46, L31

Yaqoob, T. et al., 1994a, PASJ, 46, L49

Yaqoob, T. et al., 1994b, PASJ, 46, L173

Yaqoob, T., Edelson, R., Weaver, K. A., Warwick, R. S., Mushotzky, R. F., Serlemitsos, P. J., and Holt, S. S., 1995, ApJ, 453, L81

Weaver, K. A., Nousek, J., Yaqoob, T., Hayashida, K., and Murakami, S., 1995, ApJ, 451, 147

Weaver, K. A., Nousek, J., Yaqoob, T., Mushotzky, R. F., Makino, & Otani, C., 1996, ApJ, 458, 160

Weaver, K., Yaqoob, T., Mushotzky, R. F., Nousek, J., Hayashi, I. and Koyama, K., 1997, ApJ, 474, 675

Zheng, W., Binette, & Sulentic, J. W., 1990, ApJ, 365, 115

Zheng, W., Veilleux, S. and Grandi S., 1991, ApJ, 418, 196

Życki, P. T., and Czerny, N., 1994, MNRAS, 266, 653

Fig. 1.— Upper: Spectrum of Arp102B in the region of HI Hα. Taken from a 35 minute exposure at the Asiago Observatory 1.82 m. with a dispersion of 120 Å/mm (March 26, 1989 UT=0254). Lower: Same spectrum degraded to the sampling rate of an ASCA observation of FE Kα (after narrow lines subtraction). Solid line: disk model profile fitted to the Hα profile by Chen & Halpern (1989); dot-dashed line gaussian profile.

Fig. 2.— FHWM of FE Kα versus FWHM of HI Hα, in km s^{-1}. Filled circles: SIS ASCA data; filled squares: BLRG; circled filled circles: best candidate disk emitters; the star is NGC 1068 (broad Hα component visible in polarized light). The dot-dashed line is the line of equal FE Kα and HI Hα FWHM.

Fig. 3.— Plots of HI H$\alpha$and FE Kα surface emissivity, in units of ergs s^{-1} cm^{-2}, derived from our illumination models as a function of disk radius. Full line: "cold" FE Kα (iron less than 16 times ionized) emissivity; dashed line: "hot" FE Kα emissivity; dotted line: HI Hα emissivity. See text and Table 4 for model parameters. Labels identify the model as in Table 4. "Hot" iron emission has been plotted for model (2) only for clarity. Hα surface emissivity has been plotted for r $\gtrsim$ 100 R_g.

Fig. 4.— FE Kα line profile for MCG-6-30-15 as obtained by Tanaka et al. 1995. The solid line is our best Kerr disk profile model fit with $r_{in} \approx 1.25R_g$, $r_{out} \approx 20R_g$, i = 30° and power-law emissivity with spectral index p = −1.8.

Fig. 5.— Optical Hα line profiles of 15 AGN considered in this paper, after subtraction of the underlying continuum. Vertical scale is specific flux (ergs s^{-1} cm^{-2} $Å^{-1}$ × 10^{15}); horizontal scale is wavelength in Å. The thick lines show model profiles computed following Chen & Halpern (1989). Dotted lines indicate the pure broad line (narrow lines substracted). See Table 6 for model parameters.

Fig. 6.— Observations and theoretical models of the FE Kα line. *Points:* observed data for MCG-6-30-15, *dashed curve:* accretion disk fit (Tanaka et al. 1995), *solid line:* observed averaged profile for 16 sources (Nandra et al. 1997). **(a)** *thick histogram:* double-cone optically thin radial inflow of 10^4 clouds (i = 20°, i_c = 50°, r = $16R_g$: see text), *thin histogram:* same for optically thick inflow.

arXiv:astro-ph/9712336v1 29 Dec 1997

TABLE 1

TABLE OF ASCA FeK LINE DETECTIONS

IAU Code (1)	Name (2)	Type (3)	Z (4)	Fcent (5)	Fsig (6)	F(EW) (7)	Ref (8)
J0006+202	Mark 335	Sy1	0.025	6.4	···	110	12
J0017+816	S5 0014+813	QSO	3.387	6.4	nar.	<120	31
J0123−588	Fairall 9	Sy1	0.046	6.4	0.35	300-400	12
J0228+313	Mark 1040	Sy1	0.016	6.4	0.33	550	18
J0242−000	NGC 1068	Sy2	0.003	6.4/.7	0.1/.3	11-2600	21
J0413+112	3C109	RG	0.305	6.6	0.65	300	23
J0433+053	3C120	RG	0.033	6.4	0.7	330	12
J0552−074	NGC 2110	Sy2	0.007	6.4	0.1	124	22
J0558−383	EXO 0556.3-3820	Sy1	0.034	6.3	0.5	277	9
J0615+710	Mark 3	Sy2	0.014	*	*	*	20
J0913+409	IRAS 09104+4109	QSO	0.442	6.6	0.07	450	29
J0934+273	MCG -5-23	Sy3	0.044	*	*	*	28
J0945−143	NGC 2992	Sy1.9	0.008	6.4	0.03	514	16
J0955+690	NGC 3031	Sy1	0.000	6.6/.9	0.2/.4	170-220	8
J1016+734	NGC 3147	Sy2	0.010	6.3/.6	···	370-700	19
J1023+198	NGC 3227	Sy1	0.003	6.4v	0.1/.3	250	13
J1034+396	RE J1034+393	Sy1	0.042	6.8	···	890	17
J1106+725	NGC 3516	Sy1	0.009	6.1	0.6	340	12
J1119+213	PG 1116+215	QSO	0.177	6.9	0.4	280	4
J1139−377	NGC 3783	Sy1	0.009	6.3	0.7	360-510	12, 15
J1203+445	NGC 4051	Sy1	0.002	6.0	0.1	160	10
J1210+394	NGC 4151	Sy1.5	0.003	6.4	0.7-0.9	300-400	2
J1214+140	PG 1211+143	QSO	0.085	6.6	0.48	198	24
J1218+298	Mark 766	Sy1	0.012	6.0	0.7	550	12
J1218+473	NGC 4258	Sy3	0.002	6.5	0.2	250	27
J1229+020	3C 273	QSO	0.158	6.4	0.1	19	26
J1239−053	NGC 4593	Sy1	0.009	6.35	···	90	12
J1305−495	NGC 4945	Sy	0.002	*	*	*	30
J1335−342	MCG -6-30-15	Sy1	0.008	6.4v	0.2-0.7	210-330	1
J1349−303	IC 4329A	Sy1	0.016	6.3	0.1-0.5	80-230	3
J1417+251	NGC 5548	Sy1	0.017	6.1	0.5	154	2
J1504+104	Mark 841	Sy1	0.036	6.4	0.63	580	12
J1800+666	NGC 6552	Sy2	0.026	6.4	···	300-900	25
J1836−594	IRAS 1832-5926	Sy2	0.019	6.8	0.85	580	6
J1842+797	3C 390.3	RG	0.057	6.3	0.15	190	5
J1942−103	NGC 6814	Sy1	0.006	6.3	0.6	1100	12
J2044−107	Mark 509	Sy1	0.035	6.4	0.47	200-300	12
J2235−260	NGC 7314	Sy1	0.005	6.2	0.87	458	11
J2303+088	NGC 7469	Sy1	0.017	6.3/.9	0.15	120-200	14
J2304−086	MCG -2-58	Sy1	0.047	6.2	0.35	340	7

NOTE.— Col. (1) - abbreviated (2000) position taken from the 7th edition of the Veron & Veron catalog; Col. (2) - a common name for the source as used in the ASCA-related literature; Col. (3) - AGN type; Col. (4) - optically determined redshift; Col. (5), (6), and (7) - the derived Fe Kα line peak centroid energy, profile Gaussian width (keV) and EW (eV), respectively; Col. (8) - reference(s) to the source of the Fe Kα parameters given in the three previous columns. *: objects with clear multicomponent FeK line profiles, see references for details.

REFERENCES.— 1: Tanaka et al., 1995; 2: Yaqoob et al., 1995; 3: Mushotzky et al., 1995; 4: Nandra et al., 1997; 5: Eracleous et al., 1996; 6: Iwasawa et al., 1996a; 7: Weaver et al., 1995; 8: Ishisaki et al., 1996; 9: Turner et al., 1996; 10: Mihara et al., 1994; 11: Pounds et al., 1994; 12: Nandra et al., 1997; 13: Ptak et al., 1994; 14: Guainazzi et al., 1996; 15: George et al., 1995; 16: Weaver et al., 1996; 17: Pounds et al., 1995; 18: Reynolds et al., 1995; 19: Ptak et al., 1996; 20: Iwasawa et al., 1994; 21: Ueno et al., 1994; 22: Hayashi et al., 1996; 23: Allen et al., 1997; 24: Yaqoob et al., 1994a; 25: Fukuzawa et al., 1994; 26: Yaqoob et al., 1994b; 27: Makishima et al., 1994; 28: Weaver et al., 1997; 29: Fabian et al., 1994; 30: Done et al., 1996, ApJ; 31: Elvis et al., 1994.

TABLE 2

JOURNAL OF Hα LINE PROFILE OBSERVATIONS

IAU Code (1)	Name (2)	Date (3)	UT (4)	ET (5)	Obs. (6)	Tel. (7)	Spectr. (8)	Grat. (9)	Res. FWHM (10)
J1106+725	NGC 3516	Mar. 24, 1989	21:53	2400	Asiago	1.82m	B&C	600 gr/mm	4
J1210+394	NGC 4151	Mar. 24, 1989	00:42	1800	Asiago	1.82m	B&C	600 gr/mm	4
J1239−053	NGC 4593	Apr. 2, 1990	06:03	3600	ESO	1.52m	B&C	1200 gr/mm	2
J1335−342	MCG -06-30-15	Feb. 3, 1995	11:39	2400	SPM	2.12m	B&C	1200 gr/mm	2
J1504+104	Mark 841	May 21, 1993	04:13	3300	ESO	1.52m	B&C	1200 gr/mm	2
J1942−103	NGC 6814	May 23, 1993	06:37	1800	ESO	1.52m	B&C	600 gr/mm	4
J2044−107	Mark 509	May, 25, 1993	09:33	3600	ESO	1.52m	B&C	600 gr/mm	4
J2303+088	NGC 7469	Aug. 20, 1990	10:28	1200	SPM	2.12m	B&C	600 gr/mm	4
J2304−086	Mark 926	Sept.26, 1989	03:12	3000	ESO	1.52m	B&C	1200 gr/mm	2

NOTE.— Col. (1) - abbreviated IAU designation; Col. (2) - other name; Col. (3) - date of observation; Col. (4) - universal time of observation; Col. (5) - exposure time in seconds; Col. (6) - observatory; Col. (7) - telescope; Col. (8) - spectrograph; Col. (9) - grating; Col. (10) - resolution FWHM (in Å).

TABLE 3

BROAD Hα LINE PROFILES

IAU Code (1)	Name (2)	S. T. (3)	EW (4)	FWHM (5)	Δ(FWHM) (6)	$v_r(1/2)$ (7)	Δv_r (8)	Ref. (9)
J0006+202*	Mark 335	Sy1	490	1600	300	300	100	1,2
J0123−588*†	Fairall 9	Sy1	420	4550	500	410	200	3
J0228+313	Mark 1040	Sy1	305	2200	300	0	200	4,5
J0242−000♣	NGC 1068	Sy2	···	4100	1000	···	···	6
J0433+053*†	3C 120	RG	470	2400	300	110	100	7
J0558−383	EXO 0556.3-3820	Sy1	760	4250	400	-160	100	8
J0913+409	IRAS 0910	QSO	···	···	···	···	···	···
J0955+690	NGC 3031	Sy1	26	3400	350	-140	200	9,10
J1023+198*†	NGC 3227	Sy1	285	4000	400	70	100	7
J1034+396	ZW 212.025	Sy1	200	1800	200	0	200	11
J1106+725*†	NGC 3516	Sy1	150	5300	500	-270	100	12
J1119+213†	PG 1116+215	QSO	340	2750	400	60	100	7
J1139−377*†	NGC 3783	Sy1	440	3050	300	40	100	3
J1203+445*	NGC 4051	Sy1	···	1000	200	100	100	5
J1210+394*	NGC 4151	Sy1.5	240	6400	600	-350	100	12
J1214+140†	PG 1211+143	QSO	390	1700	300	-30	100	7
J1218+298*	Mark 766	Sy1	♠195	1600	200	0	200	13,14
J1229+020	3C 273	QSO	613	3400	400	100	100	15,2
J1239−053*†	NGC 4593	Sy1	250	3400	400	-180	70	12
J1335−342*†	MCG -6-30-15	Sy1	160	2200	200	50	100	12
J1349−303*†	IC 4329A	Sy1	515	5000	400	330	150	16
J1417+251*†	NGC 5548	Sy1	540	5450	300	-590	200	3
J1504+104*†	Mark 841	Sy1	470	5000	400	-220	100	12
J1842+797	3C 390.3	RG	450	12000	1000	300	150	12,7
J1942−103*†	NGC 6814	Sy1	50	5600	1000	360	200	12
J2044−107*†	Mark 509	Sy1	550	3200	400	-200	100	12
J2303+088*†	NGC 7469	Sy1	380	2950	300	320	100	12
J2304−086*†	Mark 926	Sy1	800	7650	1500	790	300	12

NOTE.— Col. (1) - IAU code name; Col. (2) - source name; Col. (3) - Seyfert type; Col. (4) - EW in Å; Col. (5) - FWHM in km/s; Col. (6) - uncertainty at $2\times\sigma$ confidence level; Col. (7) - centroid line shift (at half maximum) in km s^{-1}; Col. (8) - line centroid uncertainty; Col. (9) - reference code. *: objects studied by Nandra et al. 1997; †: Hα profile shown in Fig. 2; ♣: broad component revealed in polarized light; ♠: estimated as EW(Hβ) × Balmer decrement.

REFERENCES.— 1: Shuder, 1981; 2: Cassidy & Raine, 1993; 3: Marziani et al., 1996; 4: Rafanelli & Schulz, 1983; 5: Osterbrock & Shuder, 1982; 6: Antonucci & Miller, 1985; 7: G. Stirpe, private communication & unpublished thesis work; 8: Morris & Ward, 1989; 9: Filippenko & Sargent, 1988; 10: Ho, Filippenko & Sargent, 1995; 11: Puchnarewicz et al., 1995 12: this work; 13: Osterbrock & Pogge, 1985; 14: Gonzalez-Delgado & Perez, 1996; 15: Morris & Ward, 1988; 16: Marziani, Calvani, & Sulentic, 1992.

TABLE 4
Explorative Photoionization Computations

Source	log L(Fe Kα)		Fe Ionization	$\log_{10}$(Hi Hα)
	$A(Fe)_\odot$	$10\times A(Fe)_\odot$		
(1)	(2)	(3)	(4)	(5)
BLR	39.65	40.50	II	41.5
Warm Absorber	39.22	40.24	IX	40.0
Coronal gas	$\gtrsim$ 35.7	$\gtrsim$ 38.2	XXVII	32.4
Dusty torus	$\lesssim$ 38.85	$\lesssim$ 39.28	IV	... [a]

Note.— Col. (1) - possible origin for Fe Kα line emission; Col. (2) and (3) - the Fe Kα luminosity computed in the case of gas with solar chemical abundances and of a factor 10 iron overabundance; Col. (4) - the dominant ionization stage of iron; Col. (5) - the expected Hi Hα luminosity.

[a] L(Hi Hα) cannot be reliably predicted by an optically thin torus model.

TABLE 5
Disk Model Results for MCG -06-30-15

Model (1)	$r_{halo,in}$ (2)	$r_{halo,out}$ (3)	τ_{es} (4)	τ_{es} Halo (5)	Continuum (6)	$\log_{10}$L(Fe Kα) (7)	$FeII_{Hot}/FeII_{cold}$ (8)	$\log_{10}$L(Hi Hα) (9)
(1)	1.	100.	0.25	0.25	MF97	41.86	$\lesssim$ 0.3	41.62
(2)	1.	100.	0.25	–	MF97	41.36	0.1	40.63
(3)	1.	100.	0.25	0.25	power-law	40.56	negligible	39.37

Note.— Col. (1) - identification number for each model; Col. (2) (3), (4) and (5) - the inner and outer radii, the electron scattering optical depth for the inner sphere and the outer halo; Col. (6) - the shape of the continuum; Col. (7), (8) and (9) - the logarithms of the Fe Kα luminosity from cold iron emission, the ratio $L(Fe\ K\alpha)_{Hot}/L(Fe\ K\alpha)_{Cold}$, and the log(L(Hi Hα)) respectively.

TABLE 6
Broad Hα Disk Model Fitting Results

IAU Code (1)	Name (2)	R_{out} (3)	$i_{opt}[1]$ (4)	$\chi^2[1]$ (5)	$i_{opt}[2]$ (6)	$\chi^2[2]$ (7)	i_{Fe} (8)
J0123−588	Fairall 9	1.0×10^5	36°	6.16	15°	0.90	89°
J0433+053	3C 120	1.9×10^5	34°	1.00	9°	1.58	88°
J1023+198	NGC 3227	1.0×10^5	36°	4.88	12°	0.81	21°
J1106+725	NGC 3516	1.5×10^5	36°	9.96	20°	1.63	26°
J1139−377	NGC 3783	2.0×10^5	50°	1.00	12°	2.25	26°
J1210+394	NGC 4151	1.5×10^5	50°	9.44	25°	1.38	24°
J1239−053	NGC 4593	1.0×10^5	38°	1.36	14°	0.76	0°
J1335−342	MCG-6-30-15	1.0×10^6	13°	0.46	9°	2.95	34°
J1349−303	IC 4329A	1.0×10^5	36°	13.6	12°	5.24	10°
J1417+251	NGC 5548	1.0×10^5	37°	7.64	18°	0.25	10°
J1504+104	Mark 841	1.0×10^5	38°	4.36	17°	0.83	26°
J1942−103	NGC 6814	1.0×10^5	38°	0.67	19°	0.1	...
J2044−107	Mark 509	1.0×10^5	35°	4.64	12°	7.08	89°
J2303+088	NGC 7469	9.0×10^5	50°	1.04	10°	0.97	20°
J2304−086	Mark 926	1.0×10^5	38°	35.0	26°	2.77	26°

Note.— All objects studied by Nandra et al. 1997 and with Hα profile shown in Fig. 5. Col. (1) and (2) - IAU code and common name; Col. (3) - disk outer radius; Col. (4) - Hi Hα disk inclination from our model 1 fits; Col. (5) - the reduced χ^2; Col. (6) - Hi Hα disk inclination from our model 2 fits; Col. (7) - the reduced χ^2; Col. (8) - Fe Kα disk inclination; data taken from Nandra et al. (1997) for Kerr geometry with reflection: in cases where multiple observations were presented, we chose the inclination with the smallest uncertainty.